STARS

Electronic Theses and Dissertations, 2004-2019

2014

Perovskite catalysts enhanced combustion on porous media and thermoelectric power conversion

Manuel Robayo
University of Central Florida

STARS Citation

PEROVSKITE CATALYSTS ENHANCED COMBUSTION
ON POROUS MEDIA AND THERMOELECTRIC
POWER CONVERSION

by

MANUEL DAVID ROBAYO
B.S. University of Central Florida, 2012

A thesis submitted in partial fulfillment of the requirements
for the degree of Master of Science
in the Department of Mechanical & Aerospace Engineering
in the College of Engineering & Computer Science
at the University of Central Florida
Orlando, Florida

Spring Term
2013

Major Professor: Nina Orlovskaya

ABSTRACT

A combustion chamber incorporating a high temperature porous matrix was design and tested. The effects and merits of combining combustion on porous media and catalytic enhancement were explored, in addition to the proof of concept of integrating these technologies with simple heat engines, such as thermoelectric generators, to generate efficient and reliable power. The direct observation of the flame during the combustion becomes possible due to a specially designed stainless steel chamber incorporating a quartz window where the initiation and propagation of the combustion reaction/flame was directly visible. The simple design of the combustion chamber allowed for a series of thermocouples to be arranged on the central axis of the porous media. With the thermocouples as output and two flow controllers controlling the volumetric flow of fuel and air as input, it was possible to explore the behavior of the flame at different volumetric flow ranges and fuel to air ratios. Additionally the design allowed for thermoelectric modules to be placed in the walls of the combustion chamber. Using combustion as a heat source and passive fins for cooling, the device was able to generate enough power to power a small portable electronic device.

The effects of La-Sr-Fe-Cr-Ru based perovskite catalysts, on matrix stabilized combustion in a porous ceramic media were also explored. Highly porous silicon carbide ceramics are used as a porous media for a catalytically enhanced superadiabatic combustion of a lean mixture of methane and air. Perovskite catalytic enhancement of SiC porous matrix with $La_{0.75}Sr_{0.25}Fe_{0.6}Cr_{0.35}Ru_{0.05}O_3$, $La_{0.75}Sr_{0.25}Fe_{0.6}Cr_{0.4}O_3$, $La_{0.75}Sr_{0.25}Fe_{0.95}Ru_{0.05}O_3$, $La_{0.75}Sr_{0.05}Cr_{0.95}Ru_{0.05}O_3$, and $LaFe_{0.95}Ru_{0.05}O_3$ were used to enhance combustion. The flammability limits of the combustion of methane and air were explored using both inert and

catalytically enhanced surfaces of the porous ceramic media. By coating the SiC porous media with perovskite catalysts it was possible to lower the minimum stable equivalence ratio and achieve more efficient combustion.

To my younger self, who dreamed of becoming an engineer

And to my family and friends

Whose love and support got me here

ACKNOWLEDGMENTS

TABLE OF CONTENTS

LIST OF FIGURES

LIST OF TABLES

CHAPTER 1: INTRODUCTION

Combustion in porous media, or matrix-stabilized combustion, refers to the technique of burning a mixture of fuel and air within a solid porous high-temperature material matrix, usually a ceramic [1-5]. This type of combustion differs from combustion in an open-flow process mainly because the thermal properties of the fluid gaseous medium and the solid porous matrix are vastly different. The thermal conductivity of the solid matrix is many orders of magnitude higher than that of the gaseous mixture, and this creates an enhanced conduction-heat-transfer along the solid of the porous medium. The high surface area of the porous solid creates an ideal medium to absorb the radiation heat from the reactants, thus raising the temperature of the solid. Additionally, the higher heat capacity in the solid porous matrix creates a 'reservoir of heat' within the combustion chamber, which would otherwise not be possible to create in a combustion chamber only filled with a gaseous mixture. The thermal and geometric properties of the solid porous matrix thus create excellent avenues for heat transfer threw convection, radiation, and conduction to recirculate the heat from the high temperature reactants back into the incoming cold gaseous products without the need of an external heat exchanger [6-9].

Catalytic enhanced combustion refers to the reaction between fuel, oxidant, and a catalytically active solid surface where the surface increases the speed of the chemical reaction between the fuel and the oxidant without itself being consumed [10]. Reactions where both the reactants and the products exist in a single phase (gaseous) are known as homogeneous; in this type of reaction, reactant molecules need to collide with one another with sufficient energy to initiate a reaction. Catalytically enhanced reactions are known as heterogeneous as the catalyst is usually in a solid phase, while the reactants are gaseous. For reactions involving the catalysts to occur, the gaseous molecules needs to be absorbed into an active site in the surface of the solid,

react, and then be desorbed back into the fluid. The high surface area of a solid porous media used in matrix stabilized combustion is very desirable as it serves as an excellent support for catalytically active sites.

The main goal of this work is to review, test, and couple two advanced combustion techniques: combustion in porous media and catalytic combustion. The objective of this work is to increase the reaction rate of premixed methane and air, increase combustion efficiency, and decrease the minimum possible equivalence ratio that a combustion chamber could achieve.

CHAPTER 2: LITERATURE REVIEW

2.1 Combustion

In his book Advanced Combustion Methods, Felix J. Weinberg outlined the reasons to employ different combustion strategies [11]. He explained that by burning near stoichiometric conditions, the maximum reaction rate is achieved, which can hold the flames stable against large flow velocities, i.e., preventing surpassing the flow velocity at which a stable flame cannot be sustained, where blowoff occurs. Although the high temperatures achieved during stoichiometric combustion are desirable, the high-temperature products created at near stoichiometric conditions, such as NO_x pollutants, are not. Thus, it is necessary then to cool the product gases down by diluting them with secondary air to reduce undesirable pollutants. By inserting excess air, other kinds of problems are created: the thermodynamic potential of high temperature for energy conversion is reduced, and there is potential for low flame stability, extinction, and low reaction rates [12].

Thus, it is necessary then to increase the reaction rates with different combustion techniques, which would allow for increasing the thermodynamic thermal potential while burning a lean mixture of fuel and air. In this work, we explore combustion in porous media that has been catalytically enhanced by high-temperature perovskite catalysts. Both combustion in porous media and catalytic combustion increase the reaction rate in combustion.

$$CH_4 + 2(O_2 + 3.76N_2) \rightarrow CO_2 + 2H_2O + 7.5N_2 \qquad (1)$$
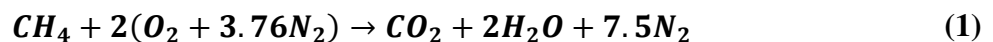
Equation (1) is the chemical equation for stoichiometric or theoretical combustion of methane and air. In this equation, air is being represented as the mixture of oxygen and nitrogen. Theoretical combustion is the combustion process of a stoichiometric mixture, a mixture where

the fuel to air ratio is such that, during combustion, all the reactants are consumed, and there is neither reactant deficiency nor excess of reactants in the reaction.

Combustion efficiency is defined as the fraction of the available heat in the mixture to the heat that is released in the reactant by the combustion reaction, which is dependent on complete combustion of the fuel; incomplete combustion products, such as CO, imply lower combustion efficiency [11, 13]. With the use of a gas chromatograph, it is possible to measure the combustion efficiency as it is inversely proportional to the ratio of unburned gases, leaving the systems to the mixture entering it. See equation (3).

$$\boldsymbol{\eta = 1 - \frac{\mu_{unburned\ exhaust}}{\mu_{incoming\ fuel}}} \tag{2}$$

The composition of the gaseous mixture under combustion, the amount of fuel and air of the mixture, can be referred to in terms of equivalence ratio, which is the fraction of the fuel and air of the mixture divided by the same ratio under stoichiometric conditions.

$$\Phi = \frac{m_{fuel}/m_{air}}{\left(m_{fuel}/m_{air}\right)_{stoich}} \tag{3}$$

Thus, as seen in equation (3), a mixture that has enough oxidant to burn the fuel completely without excess oxygen left is said to have an equivalence ratio of 1.0. If the equivalence ratio is above one, meaning that there is not enough oxidant to react will all the fuel, the mixture is said to be rich. Similarly, if the mixture is below one, meaning there is excess air (oxidant) in the products, then the reacting mixture is said to be lean. The lean limit is defined as the least fuel content at which the mixture will burn, while the rich limit is reach when the fuel content in a mixture is high enough to create a composition deficient of oxygen [11]. The firing rate is defined by the inlet velocity and the lower heating value of methane [14], with [kW/m^2]

4

as units. The flow velocity and the equivalence ratio of a mixture are enough to define its firing rate.

$$k(T) = A\ exp(-E_A/R_uT) \tag{4}$$

Equation (4) is an empirical formula of the bimolecular rate coefficient, and this equation is remarkably accurate at predicting the temperature dependent of reaction rates. Where A is a constant term, the pre-exponential factor, or the frequency factor, E_A expresses the fraction of collisions that occur with an energy level above the threshold level necessary for reaction, or the activation energy [J/kmol]. R_u is the universal gas constant [J/kmol K], and T is temperature in (K) [10]. Combustion on porous media increases the reaction, k, rate by increasing T, without changing the mixture's fuel to air ratio, to one nearing stoichiometric conditions. While catalytically enhanced combustion increases k by giving the products an alternative pathway of reactions to complete combustion, reducing the E_A needed to initiate the reaction.

2.1.1 Combustion inside porous media

Excess enthalpy combustion was first described in 1971 in a *Nature* article titled "Combustion Temperature: The Future?" In this article, F. J. Weinberg described methods of recirculating the heat from the reactants back into the products by using an external heat exchanger that preheated incoming reactants [15]. An alternative means of achieving excess enthalpy combustion is to insert a porous solid with superior heat transfer properties into the combustion chamber [1]. In literature, combustion in porous media could be broken down in two categories: excess enthalpy combustion where the flame is stationary and stabilized in a fixed region of the porous media and super-excess enthalpy or superadiabatic combustion [16, 17]. The superadiabatic effect refers to when both the thermal wave and the reaction move through

the porous bed in the same direction, and velocity, coinciding, is in a transient propagating combustion zone within the porous media. The energy released can more than compensate for energy losses from the thermal wave, which will act as a high-temperature bath for the reactions, thus increasing the final temperature of the flames above the normal adiabatic temperature of combustion[9].
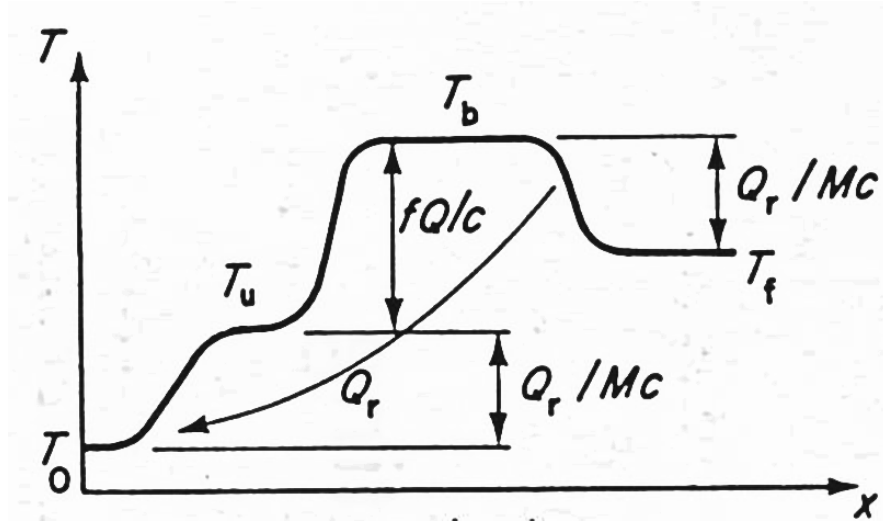
Figure 1. Schematic temperature profile in heat recirculating burners [11].

By the use of an external heat exchanger, or porous ceramic media within the combustion chamber, it is possible to create a "reservoir of heat" that is driven by the recirculated thermal energy from the combustion reaction products. Allowing the incoming reactants to release their chemical energy at the highest energy point [15]. By using heat recirculation techniques, it is possible to raise the enthalpy of the mixture higher than the total enthalpy of the initial state of the reactants plus the heat of combustion of the fuel. In Figure 1, Q_r represents the recirculated heat of combustion, M represents mass flow, c represents the mean specific heat at constant pressure of the mixture, and finally, fQ/c where f is the fraction of stoichiometry and Q is the heat of combustion. Under a normal combustion, the final enthalpy of a mixture of fuel and air will be lower than the enthalpy of the initial state of the mixture plus the heat of combustion of

6

the fuel, or less than *fQ/c*, because no real combustor is completely adiabatic. However, under excess enthalpy combustion, it is possible to achieve a *fQ/c*+ Q_r as seen in Figure 1. This method of 'borrowing' enthalpy from the combustion products to preheat the incoming reactants is referred to as 'excess enthalpy combustion' [1]. Thus, excess enthalpy combustion is a very novel way of increasing the enthalpy of the products at a given point in the combustion chamber without having to change the reactant composition.

The recirculation of heat from the products into the reactants in high-temperature porous ceramics can result in local temperatures higher than the adiabatic flame temperature for a given mixture. This effect is referred to as super adiabatic combustion. Zhdanok et al. has reported a maximum temperature observed using this combustion technique as ~2.8-fold higher than the normal adiabatic temperature for the same mixture. In his experiment, the filtration combustion waves propagated at very low velocity (~10^{-3} cm/s) [9].This combustion technique increases the burning rates of gas mixtures, allows for the combustion of low calorific gas mixtures, and creates large thermal gradients in the porous solid matrix [18]. This allows for the design of burners with high power density, high power dynamic range, and very small emission products [19].

Takeno and Sato were the first to demonstrate this concept analytically [4] and experimentally [20].They proposed producing an excess enthalpy flame by inserting a porous solid of high thermal conductivity into the combustion zone, creating a one-dimensional flame zone model to test the effects of such a technique and investigate the effects of the mass flow rate and the heat transfer coefficient on the flame characteristics.
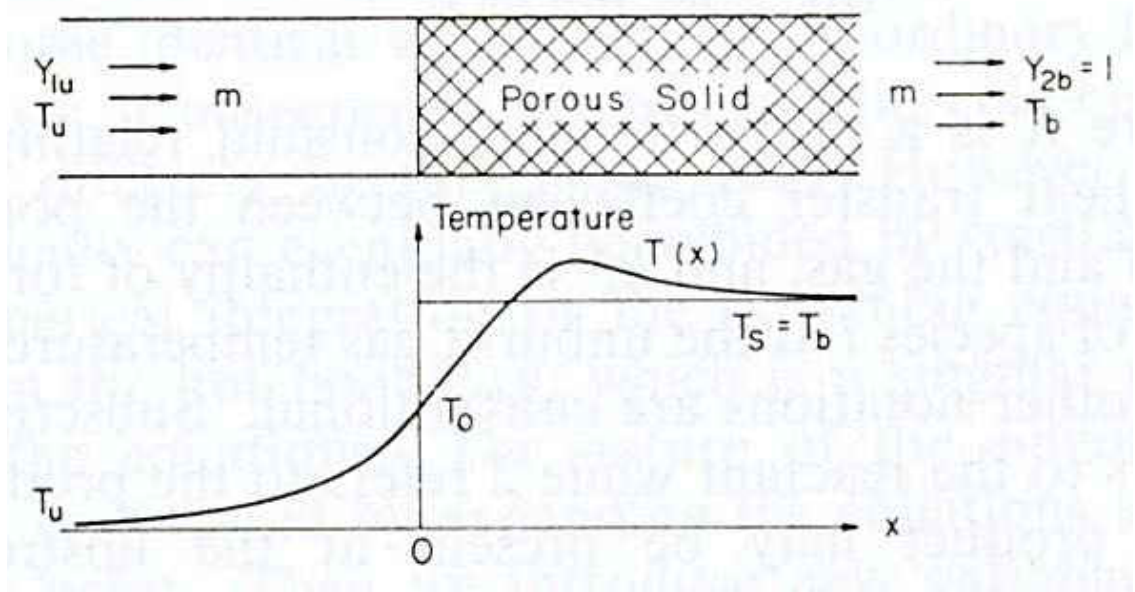
Figure 2. Schematic representation of adopted flame model[4].

In the Takeno and Sato model (see Figure 2), most of their assumptions were identical to those of the ordinary flame theory, with the exception of the energy conservation, which contained the addition of the heat flow from the solid, see equation (5).

$$\frac{d}{dx}\left(\lambda\frac{dT}{dx}\right) - mc_p\frac{dT}{dx} + K(T_s - T) + \left(h_1^{\circ} - h_2^{\circ}\right)w_2 = 0 \tag{5}$$

In equation (5), most of the notations are conventional with the exception of K, which is the proportionality constant relating to the heat transfer coefficient between the gas and the solid, and h_1° is the enthalpy of formulation of species I at the unburnt gas temperature. The first term is the heat transfer rate, with λ being the thermal conductivity of the fluid. The second term is a convective term. The third term refers to the energy transfer between the fluid and the solid. The final term refers to the energy produced per production rate of the species by chemical reaction, w_2. Takeno and Sato concluded that the flame structure can be controlled by heat transfer coefficient between solid and the gas. This coefficient is a function of the total surface area of the porous solid; thus, it can be controlled by changing the porosity in the solid. The increase in

temperature due to heat recirculation did not increase the amount of NO_x produced as the temperature peak was too sharp, and the stay time in the region was too short. The most significant result from their model was that the flame could sustain an increased mass flow rate, ten times as large as the burning velocity, just by inserting a porous solid in the combustion chamber.

A later model by Takeno and Sato with a finite length solid revealed that there is a critical flow rate above which the system, composed of a porous solid matrix of finite length, cannot sustain combustion. However, by increasing the length of the porous solid, the critical mass flow rate would increase by almost the same factor [20].

V.S. Babkin described the velocity of the thermal wave used in combustion on porous inert media for excess enthalpy applications as combustion in low-velocity regime [8]. In this application, steady state wave velocity depends on the properties of both the gases and the inert porous media. Depending on the flow velocity and other parameters, the steady state combustion can move with the flow, against it, or stand still. The heat recirculation is a function of the direction and velocity of the wave, e.g., a wave that propagates downstream gives rise to a new convective heat flow due to its relative motion to the solid. Thus, the efficiency of a recuperation cycle increases [8]. There are two main mechanisms of flame propagation. The first is very close to normal combustion (referred as high-velocity combustion), where propagation of the flame is dictated by the thermal conductivity of the gases, and the thermal interaction between the solid and the fluid mixture is not important. The second mechanism (low-velocity combustion) is characterized by extensive heat exchange between the solid porous media and the fluid [9].

Trimis and Durst were the first to design a burner with a preheating lower porosity section that prevented the flame from propagating downstream followed by a higher porosity

9

section where the flame could be successfully stabilized [19]. Trimis and Durst reported that for the flame to stabilize successfully on the porous matrix, the average pore diameter had to be large enough to allow a modified Peclet-number to be higher than (Pe>65) so that quenching of the flame inside the porous ceramic matrix does not occur [19]. Where the limiting Peclet number for the flame propagation in porous media is defined by the following equation:

$$Pe = \frac{S_L d_m c_p \rho}{\lambda} \tag{6}$$

In equation (6), S_L is the laminar flame velocity, d_m is the equivalent porous cavity diameter, c_p is the specific heat capacity, ρ is the density, and λ is the heat conductivity of the gas mixture. This work is important in porous burner design as it allows for the creation of a ceramic of lower porosity section at the inlet of the combustion chamber that prevents flashback of the flame, followed by a larger porosity section where the flame can be successfully stabilized. The thickness of this lower porosity ceramic section, located upstream from the reaction, plays a small factor on the heat recirculation but does not otherwise significantly affect the performance of the burner [14], and it can be rather thin for practical purposes. Additionally, Trimis and Durst derived the following conclusions about porous media:

- Porous media burners can have 10-15 lower volume than existing external heat exchanger burners.
- Porous media burners have a high power dynamic range of 20:1.
- Stable combustion is possible for a wide range of gas properties and a wide range of air/fuel ratios.
- The system is insensitive to variations and gas mixture properties.

Mital et al. were the first to measure the temperature and species profiles within the submerged reaction zone of a reticulated porous ceramic matrix [21]. The main goal of their research was to provide fundamental information concerning the structure of nonadiabatic (sub-adiabatic) flames to validate previous models. They conducted measurements of stability range, radiation efficiency, and pollutant indices. Additionally, they were the first to document how the reaction zone moves upstream as the firing rate is increased.

Huang et al. investigated the effects of preheating the porous media on the initiation and extinction of the flame in super-adiabatic combustion [6]. Their experimental setup and procedure allowed them to independently control the critical energy content (preheating), firing rate, and the equivalence ratio inside of the combustion chamber to test the effects of varying each of those parameters on super-adiabatic combustion. It was concluded that preheating of the solid was important to initiate and to stabilize a super adiabatic reaction, that the amount of preheating necessary was a function of both the firing rate and the equivalence ratio. The equivalence ratio has a stronger influence in the initiation of a super adiabatic reaction; the lower the equivalence ratio, the higher the amount of preheating necessary to initiate a super adiabatic reaction.

Mathis et al. investigated the operating firing rate range, the influence of the depth of the preheating section (commonly used in porous burners matrix stabilized burners), and the effects of using different articulated ceramics materials in the stabilization of the flame inside of the combustion chamber [14].
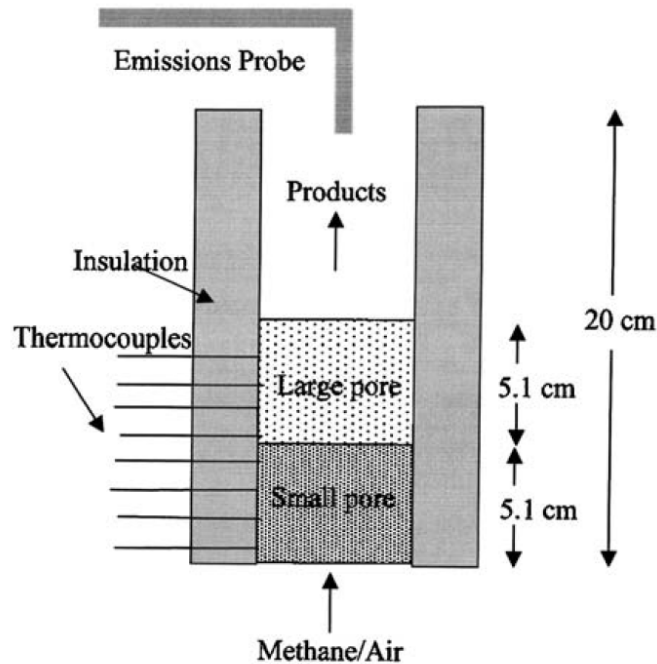
Figure 3. Sketch of porous burner. Dimensions shown are for the first YZA and the ZTM burner [14].

Figure 3 shows the schematic of the Mathis experimental setup. In this setup, the thickness of the large pore section of the porous burner, or the flame-stabilization layer, affects how much heat is recirculated within the porous media. On a thin flame-stabilization layer, most of the heat radiates to the surroundings as opposed to recirculate towards the reactants. In a thick–flame stabilization layer, heat is more effectively recirculated back into the reactants, resulting in higher flame temperature and enhanced flame speed [14]. The small pore section of the burner had 23.6 ppcm, while the large pore section had 3.9 ppcm. The diameter of the combustion chamber was 5.08 cm in diameter. In this work, it was investigated the range of the firing rate at which this burner set up could successfully stabilized a flame at different equivalence ratios for YZA and ZTM articulated ceramic burners. It was discovered that at lower firing rates, the flames tend to stabilize closer to the interface (upstream between the lower and higher pore sections), while with increasing firing rates, the flame stabilizes farther downstream

until blowoff occurs. The YZA burner successfully stabilized a flame with a firing rate of 4000 kW/m^2 at an equivalence ratio of 0.65, while the ZTM did not stabilize the flame effectively.

Zhadanok, Kennedy et al. explored further combustion in porous media, they described how the thermal energy transferred between the filtrated gas and the porous medium is a function of the filtrated flow and the combustion wave velocity [9].
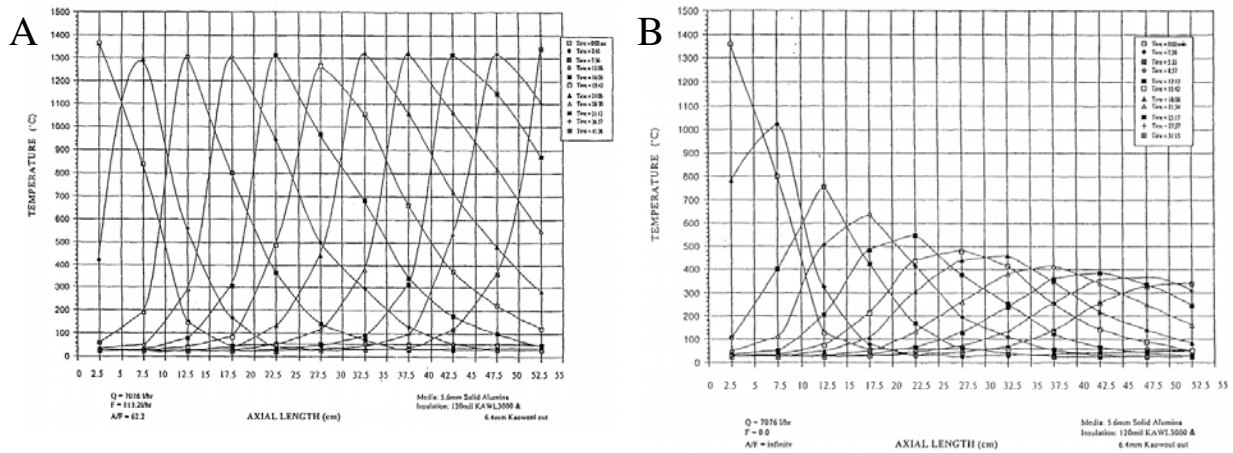
Figure 4. Shows two kinds of downstream propagating waves in the porous media: A. Stable combustion wave where both the thermal and combustion wave have coinciding velocities, and B. Decaying wave with losing amplitude. Both waves have the same initial thermal loading and equivalence ratio [9].

The filtration flow and the combustion wave velocity can create a traveling accumulation of energy inside of the solid porous media, or a thermal wave. When both the thermal wave and the reaction wave velocities coincide, the energy released by the reaction wave can more than compensate for energy losses on the thermal wave, while the thermal wave works as a high temperature bath for the reaction wave, thus increasing the thermal energy transfer between solid and gas filtration, see Figure 4. The combined wave, or resonance wave can increase the temperature of the mixture in excess of its adiabatic temperature, thus allowing for a self-propagating reaction even in a low exothermic medium [9].
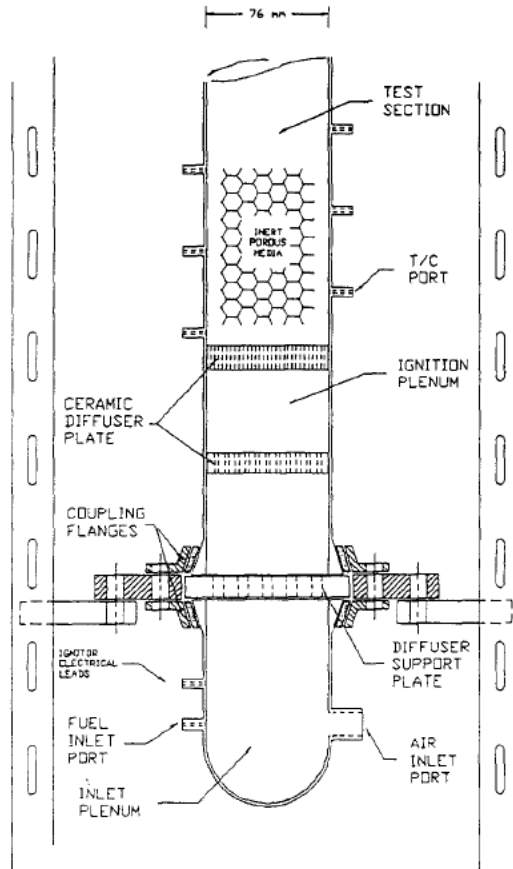
Figure 5. Zhdanok schematic of experimental apparatus [9].

Figure 5 shows the schematic configuration of the burner Zhadanok, Kennedy et al. use for this work. The quartz glass tube test section was 1.3 m in length, 76 mm in diameter, and filled with 5.6 mm alumina spheres. The walls of the quartz tube were insulated both in the internal and external diameters in order to minimize the heat losses inside the quartz tube. An array of type S thermocouples were inserted through small ports in the quartz wall and placed normal to the axis. The reaction wave propagated at approximately 2 x 10^{-3} cm/s with gas filtrating at 43 cm/s. The A/F = 62, or 0.28 equivalence ratio, was used in this experiment, which is significantly lower than the normal flammability limit. The maximum temperature in the wave was approximately 2.8 times the normal adiabatic temperature for the given air to fuel ratio.

14

The overall relationship between the combustion temperature, gas mixture filtration velocity and velocity of wave propagation is well illustrated by heat balance equation of the filtration wave [22]:

$$u/v_f = k(1 - \Delta T_{ad}/\Delta T_c) \tag{7}$$

Where u is the combustion wave propagation velocity, v_f filtration velocity, ΔT_{ad} is the adiabatic temperature of combustion, k is the constant depending on the porosity and heat properties of the packed bed, and ΔT_c is the combustion temperature. Equation (7) shows that when the fuel concentration has very little enthalpy, hence small ΔT_{ad}, the combustion wave velocity is positive and close to the thermal wave velocity. When the fuel concentration is increasing, but the adiabatic temperature is less than the combustion temperature, the super adiabatic wave propagates downstream with the velocity decreasing to zero. Combustion wave propagating upstream becomes possible when the adiabatic temperature exceeds the temperature of the combustion zone [23]. When this happens, the combustion wave cannot be classified as supper adiabatic. A standing wave exists when ΔT_{ad} is equal to ΔT_c.

2.1.2 Porous material properties and selection

Material selection is the most important part in the design of a porous burner as the material properties and geometry will dictate the performance, longevity, and versatility of the system [24]. The material matrix in porous media burners undergoes severe thermal and chemical stress during operation, created by high temperatures and steep temperature gradients in a corrosive atmosphere [25]. The material properties of the matrix will primarily dictate its susceptibility to cracking from thermal fatigue and the melting point of the combustion chamber [2].

15
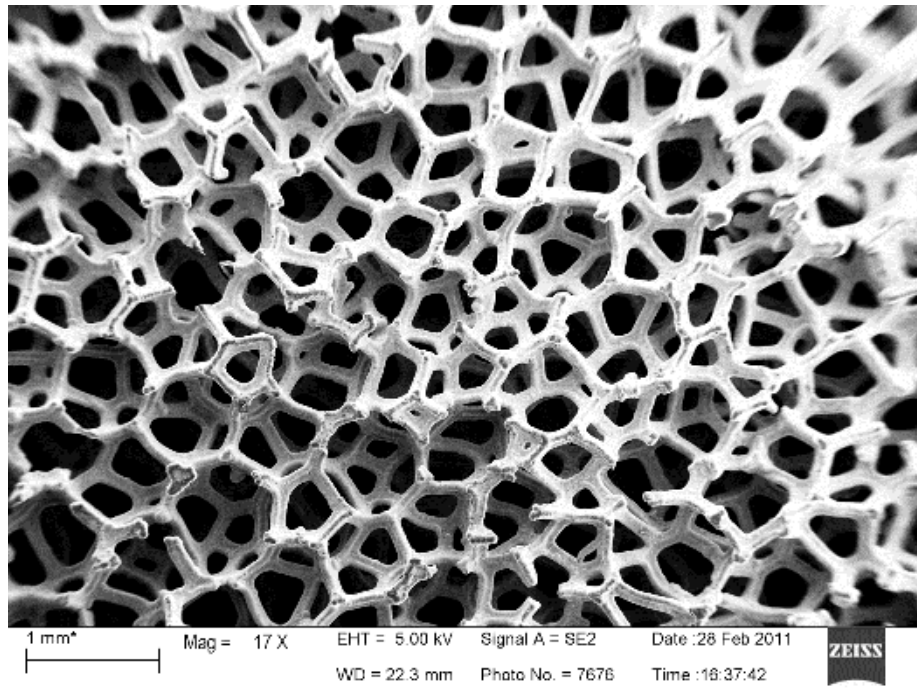
Figure 6. SiC porous media under SEM.

Combustion takes place between the cavities within the porous medium, see Figure 6. The flame exists within the voids of the porous matrix [26]. Thus, the volumetric void fraction, porosity, and average pore size typically measured in pores per centimeter (ppcm) or pores per inch (ppi) are important parameters in porous burner design. Zheng et al. tested the effect of the average pore size by changing the average pore size of a SiC porous burner [26]. The researcher varied the pore density from 10 to 30 ppi and reached the following conclusions: The preheating zone increases in length as the pore size increases due to weak convective heat transfer at 10 ppi and more intense convective heat transfer at 30 ppi; The peak temperature in filtration combustion could be affected, the maximum temperature occurred at 30 ppi due to its large specific surface area and low extinction coefficient; At 10 ppi, weak convection, while at 30 ppi, weak radioactive heat transfer was the reason for fast combustion wave propagation; and at 20 ppi, the slowest combustion wave propagation velocity occurred.

Due to their elevated temperature stability, ceramics have become the most widely used material in porous burners. Alumina (Al_2O_3), Zirconia (ZrO_2), and silicon carbide (SiC) based materials are the most commonly used in research [24]. Table 1 shows relevant material properties of Al_2O_3, ZrO_2, and SiC ceramics for combustion in porous media. These ceramics are considered inert, and no catalytic reaction is expected in their surface [2]. Recirculated yttria-stabilized zirconia/alumina (YZA) composite and zirconia-toughened mullite (ZTM) have been used in porous burner flame stabilization research [14] because of their superior maximum exposure temperature: YZA and ZTM 1870 K and 1920 K, respectively. Ceramics, are still subject to degradation after exposure to typical combustion temperatures and as a consequence of thermal cycling [14].

Table 1. Most important material data of Al_2O_3, SiC, and ZrO_2 [25].

Parameter	Dimension	Al_2O_3	SiC	ZrO_2
Max use temperature in air	°C	1900	1600	2300
Thermal expansion coefficient α (20 – 1000 °C)	10^{-6} 1/K	8	4-5	10-13
Thermal conductivity λ at 20 °C	W/mK	20-30	80-150	2-5
Thermal conductivity λ at 1000 °C	W/mK	5-6	20-50	2-4
Specific thermal capacity	J/gK	0.9-1	0.7-0.8	0.5-0.6
Thermal shock resistance, hard shock, R1 ($\sigma/E\cdot\alpha$)	K	100	230	230
Thermal shock resistance, mild shock, R'·($R\cdot\lambda$)	10^{-3}W/m	3	23	1
Total emissivity at 2000 K	-	0.28	0.9	0.31

Because of their limited performance, metallic materials are not commonly used in matrix-stabilized burners. Metals are more commonly used in surface stabilized burner applications. However, metals have high thermal capacity per unit volume, thus porous burners

made of metals have low thermal inertia [25], meaning that combustion within porous media metals is more resistant to abrupt changes in temperature or flow. Stainless steel, iron-chromium-aluminum, and nickel-based super alloys have been considered in past as suitable materials for porous burner research [2, 6].

Porous ceramic foams and discrete ceramic structures/elements are the most widely used type of porous burner structure. Reticulated porous ceramics are an attractive material because they have porosities that approach 90% porosity, thus decreasing the pressure drop [14]. Because of their high surface area to volume ratio, they are great as catalyst carriers and particle filters. Because of their geometry, they do suffer from limited thermal shock resistance since they exhibit large temperature gradients across the bulk material during the ignition and the termination of the combustion process [27].

O. Pickenacker et al. listed the advantages of articulated foams as follows: Good flow through properties reduce pressure loss due to their open structure; excellent heat transfer as the geometry increases the convective heat transfer between the structure of the media and the fluid; and finally, the structure has a very light weight, which translates into low thermal inertia, which has the effect of making the burner warm up quickly and adapt to power changes well [25]. SiC foams are a good material for combustion in porous media due to their high thermal conductivity, high thermal emissivity, low coefficient of thermal expansion, and good thermal shock resistance [2, 24, 26].

Pack beds are more adequate for use within reciprocal flow porous burners because they exhibit better thermo-mechanical stability and tolerance to thermo-cycling. Additionally utilization of packed beds with increased porosity may be effective for pressure drop reduction [28].

Three dimensional interwoven lamellae, which is made of punched, woven fiber, solid or foam is also used [2]. Finally, other structures, such as monolithic alumina with multiple pore channels or honeycomb, have been used to preheat some of the porous burner [2]. Other structures, such as fibrous structures, have been proposed for a porous burner, but have not been widely used due to their geometric properties [2].

2.1.3 Examples of ultra-lean burner performance

Afsharvahid et al. investigated the stabilization of ultra-lean methane and propane flames in porous media [29]. In this investigation, a reaction chamber was designed using a well-insulated cylindrical alumina casing filled with alumina beads. A the first layer of beads, upstream from the inlet of the burner, is 75 mm thick and consists of beads of 2 to 3 mm-diameter this layer acts as a flame arrestor. The insulated cylinder had a diameter of 15.4 cm and was 60 cm in length. The combustion chamber, where the flame was stabilized, was filled with 6 mm spheres, and was 350 mm thick. In this work, it was investigated the flow range, for both methane and propane, so that the flame could be successfully stabilized. It was possible to stabilize the flame with a flow range of 9 to 28 cm/s and an equivalence ratio as low as 0.35. The increase in flow velocity shifted the flame front downstream, and the magnitude in downstream flame shift differed from methane and propane mixtures. This was explained by the fuel density, which affects the momentum and energy balance of the mixtures.

Bingue et al. investigated the lean limit of combustion on porous media made of a packet bed of alumina spheres with a diameter of 5.6 mm. The researchers' investigated wave propagation under ultra-lean methane/air mixtures with equivalence ratios from 0.25 to 0.9 and filtration velocities from 10 to 40 cm/s. The combustion chamber consisted of a quartz tube that was 45 cm in length and 38mm in diameter. The packet bed of alumina spheres had a porosity of

19

approximately 40%. The inner lining of the quartz tube was insulated with 2 mm of insulation, while the outside of the quartz tube was insulated with 30 mm thick high-temperature insulation [22].
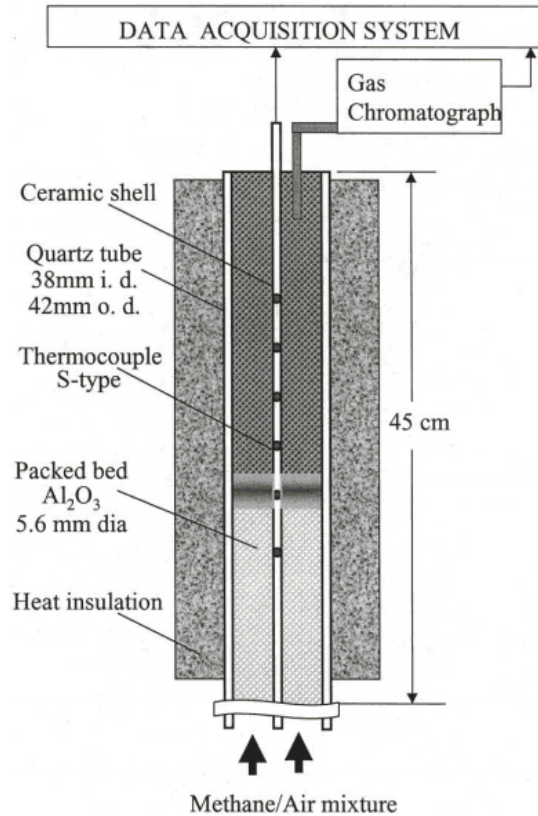
Figure 7. Kennedy's schematic of experimental apparatus[30].

In further research, with the same porous reactor but a lower flow velocity of 0.25 m/s. Kennedy et. al. was able to extend the lean limit of the porous burner to an equivalence ratio of 0.2. Additionally, the temperature, velocity, and chemical products of the combustion wave in the equivalence ratio from 0.2 to 2.5 was investigated. The researchers reported downstream (superadiabatic) wave propagation for ultralean ($\Phi \leq 0.45$) and ultrarich ($\Phi \leq 0.45$) [30].

Christo et al. with a burner of the same design as Afsharvahid reported only preliminary results where it was possible to maintain combustion at an equivalence ratio of 0.1 at a firing range of 90 kW/m^2. However, these results are taken with some skepticism in the community as

a complete set of results has not been published, and it could be possible that the observed behavior is an example of transient combustion with a very low flame speed [1, 31].

2.1.4 Reciprocal flow burners.

In 1990, Swedish engineers designed a superadiabatic reciprocating flow burner in porous media using practical experience [32]. Reciprocating combustion in porous media (RCPM) essentially works on the same principles of excess heat recirculation of traditional combustion in porous media. Due to the reciprocating flow of the burner, the flame is designed to stabilize at the center of the combustion chamber, creating a sharp trapezoidal temperature gradient inside of the combustion media as shown in Figure 8. At the beginning cycle, a temperature gradient inside of the porous media will form, in similar fashion as in unidirectional combustion in porous media, with the highest temperature within the solid downstream from the flow direction. Once the flow changes direction, the incoming mixture will encounter a solid temperature higher than the one experienced by the incoming mixture of the previous half-cycle. Thus, an accumulation of heat would result within the solid where each consecutive cycle increases the temperature encountered on the solid by the mixture, thus creating an excess enthalpy combustion chamber capable of burning extremely dilute mixtures, in addition to creating a sharp temperature gradient ideal for power generation [3, 23, 32, 33].
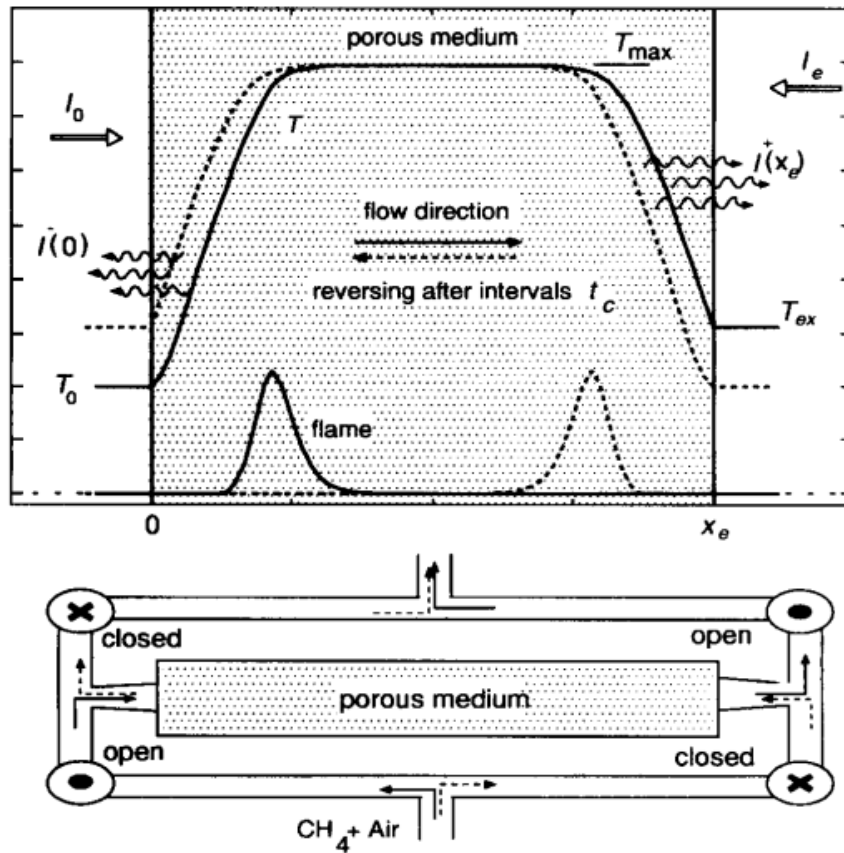
Figure 8. Schematic model of the reciprocating combustion system and the profiles of temperature T [32].

Hoffmann et al. did an experimental study on the behavior of an RCPM, and they explored the flammability limits and the NO_x and CO emissions of the system [32]. Figure 8 shows the experimental schematic of their setup. As with traditional combustion in porous media, the flow velocity and equivalence ratio have a dominant effect on the overall process since the energy input into the combustion chamber is proportional to both parameters [32].
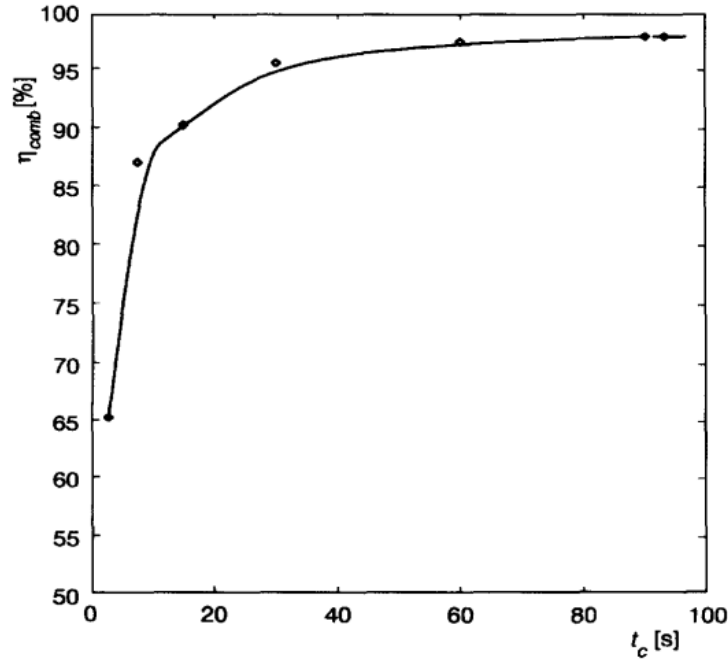
Figure 9. Combustion efficiency as a function of the half cycle time with a constant equivalence ratio of 0.096 and a flow velocity of 0.14 m/s [32].

By keeping the equivalence ratio and the flow velocity constant, Hoffmann et al. were able to measure the efficiency of the duration of the half cycle in RCPMs. Figure 9 shows the result at a given equivalence ratio and flow velocity. The efficiency of the RCPM decreases with decreasing half cycles because the time required for fresh air to exchange the burned gases becomes longer. By controlling the fuel flow and making the period of its supply shorter than half a cycle duration, it is possible to achieve 100% efficiency as fresh air will replace any combustible gases upstream of the reaction zone [32]. The porous media used in this study had a porosity of 87.5% with three different types of average pore size media: 6, 13, and 30 pores per inch. A combustion limit of an equivalence ratio of 0.028 was achieved for the fine average pore size media due to low radiation losses due to its large optical thickness.

Hanamura et al. investigated the superadiabatic combustion within a RCPM burner. They found that flame temperatures in the porous medium were 13 times higher than the theoretical

23

one of the ordinary flame-free space. With a heating value mixture of about 65 kJ m^{-3}, which would be equivalent to a temperature increase of just 50 °C [34].

Jugjai et al. investigated the application of using a RCPM as a water heater. The porous combustor heater with cyclic flow reversal combustion extracts heat directly from the porous media bed in the combustor (via pipes circulating water), by taking advantage of the trapezoidal temperature gradient inside of RCPM burners, thus creating ideal conditions for combustion augmentation and heat transfer enhancement. With an equivalence ratio of 0.65, a firing rate of 14.6 kW and a half cycle period of 185 seconds Jugjai was able to achieve a thermal efficiency of 85%, with low emissions of Co and NO$_x$ of 200 and 20 ppm, respectively [17].

Drobrego et al. did an analytical and numerical investigation of methane-air lean combustion limit inside of a RCPM burner [28]. Using an analytical model, they investigated important parameters in the design of an RCPM burner, such as heat loss coefficient, reactor length, pressure, particle size, and porosity. Additionally, they validated their model with data from Hoffmann and Hanamura [32, 34].
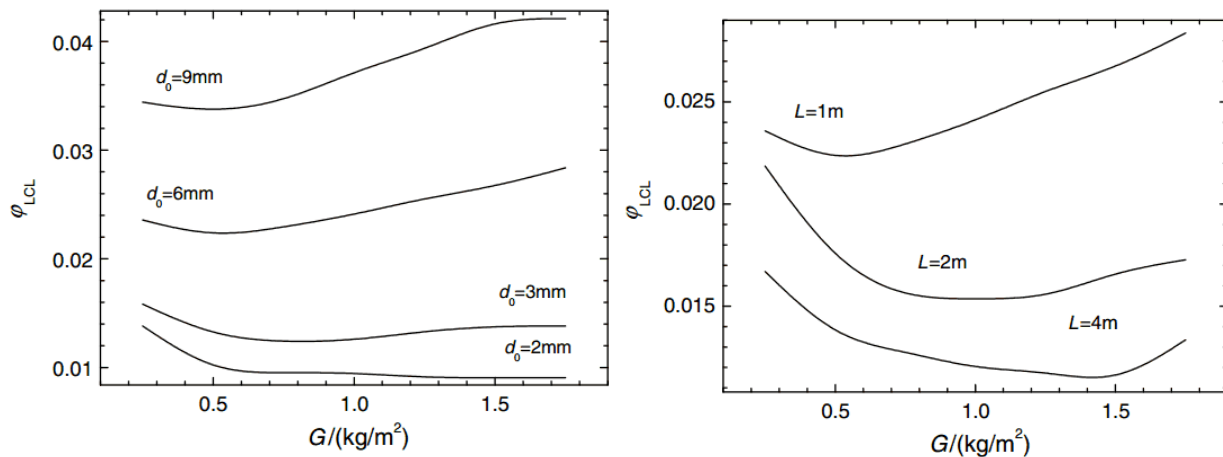
Figure 10. Equivalence ratio vs. gas mixture specific mass flow rate. Varying diameter of porous media diameter, left. Varying the length of the reactor, right [28].

24

Drobrego et al. concluded with this analytical model that the particle size is the most important factor influencing the methane-air lean combustion limits, as seen in Figure 10 on the left plot. As the reactor length increases, the methane-air lean combustion limit decreases, as seen in Figure 10 on the right plot. But a high flow rate is necessary to decrease the lean limit in a long reactor, which results in high pressure loss and pumping energy losses. By changing the outlet pressure of the reactants and small variation on porosity it did not influence the lean limit of the reactors as much as the other factors [28].

2.2 Perovskite Oxide Catalysis

Catalysis is a technology that increases the rate of chemical reaction. Catalysts change the individual steps followed in a reaction and essentially avoid those that slowed the entire reaction down by employing catalysts an alternative pathways to homogeneous fuel oxidation or oxygen reduction is formed. More specifically, catalysts are materials, which change the rate of attainment of chemical equilibrium without themselves being changed or consumed in the process [35]. Noble metals, such as platinum (Pt) or palladium (Pd), show high methane combustion activity at low temperature, and they, indeed, are very promising candidates to facilitate combustion reactions [36, 37]. However, while catalytic activity of noble metals is high, their cost is also very high, and their possible sublimation and/or sintering can occur in a catalytic burner at high temperatures in the presence of water and CO_2 gasses [38]. Another problem in the catalytic combustion of methane and other hydrocarbons is carbon deposition and, as a result, catalyst deactivation [39].

The prohibitive cost and scarcity of the noble-metal catalysts have driven research for an appropriate substitute. In addition, high temperature catalytic processes like deep oxidation/combustion of methane, partial oxidation of methane and other fuels has become very

25

attractive application. Therefore, finding appropriate catalysts that promote fuel oxidation and oxygen reduction during combustion at high temperatures has become increasingly desirable in recent years. Perovskites have promising catalytic activity at moderate temperatures even when compared with platinum-based catalysts and have good heat resistance of up about 2000°C [40]. Perovskite has shown to be effective for catalytic combustion, natural gas steam reforming, and electrochemical reactions due to their well-known thermal stability in a broad range of temperatures, as well as high oxygen storage capacity and oxygen ion conductivity[41]. Additionally, a catalyst can work efficiently in a very large concentration domain, allowing the use of lean fuel/air mixtures [42].

2.2.1 Crystal Structure

The perovskite crystal structure was first described by the geologist Gustav Rose in the 1830s. Rose named this structure after the Russian mineralogist Count Lev Aleksevich von Perovski [43], and it follows the general formula ABO_3 (see Figure 11), where A and B are metal atoms and O is oxygen [44]. The first material described with this structure was $CaTiO_3$, but it is better typified by $SrTiO_3$[45]. It has a cubic (isometric) structure with the A atom located at all eight corners of the cube, a single B atom at the center of the structure, and O^{2-} ions located at the center of each of the six faces [46].
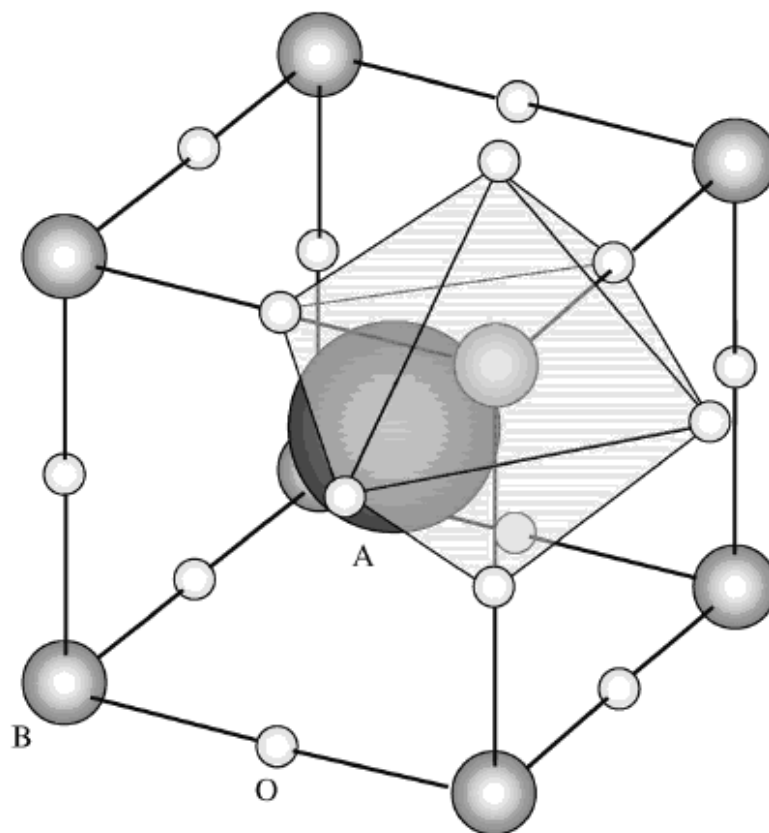
Figure 11. Structure of Perovskite (ABO3) [43].

A and O form a cubic closest packing, and B is contained in the octahedral voids in the packing (see Figure 11).

The most attractive part of using perovskites as catalysts is the high number of choices when picking A and B ions to fit into the structure. Selection of the B site ion is the most effective way of optimizing the catalytic activity of the perovskite [47]. In perovskite catalysts, the B ions may be catalytically active $3d$, $4d$, or $5d$ transition metal ions that occupy oxygen octahedrons [48]. The catalytic activity for oxidation is mainly determined by the transition metals in the B site, and the utilization of the perovskite crystal structure is mainly used to increase the thermal stability of the transition metal oxide [43]. Transition metals are considered a good catalyst for many applications. Labhsetwar et al. has synthesized a perovskite with the transition metal ion ruthenium in its B-site that has shown high catalytic activity. He synthesized

27

LaRuO$_3$ with an oxidation state of 3+, but Ru favors an oxidation state of 4+ Thus, to increase the thermal stability of the perovskite, he synthesized La$_{.35}$Ru$_{4.0}$O$_{13,}$ which has an Ru oxidation state of 4+, thus this particular perovskite composition had high thermal stability, adequate even for applications such as combustion [49].

The A site ions, which fit in the dodecahedral interstices, are categorized by large rare-earth atoms, such as Lanthanum, alkaline-earth, or other large ions, such as Bi^{3+} or Pb^{2+} [48]. LaBO$_3$ perovskite oxides may be suitable catalysts for the methane coupling reaction because they are characterized by high mobility of oxygen ions[50]. The use of Pb^{2+} as the A site ion, as in Pb$_2$Ru$_2$O$_3$, for example, protects the B site transition metal ion from lead from the exhaust, which can act as catalytic poison, in reduction of NO to N$_2$ of gases leaving an engine [48].

2.2.2 Valency and vacancy controls

Additionally, solid solutions of A'BO$_3$, AB'O$_3$, and A'B'O$_3$ substitutions insert an even higher degree of tailoring of catalytic properties for any given perovskite crystal structure. Due to these substitutions, valency, stoichiometry, and vacancy can vary widely and have very different properties than an ABO$_3$ perovskite (compared with A'BO$_3$, AB'O$_3$, and A'B'O$_3$) [39, 40, 43]. By partially substituting the A cation in the perovskite lattice with a A' cation, it is possible to deeply modify the catalytic properties by formation of oxygen vacancies, electrophilic oxygen species, or stabilization of unusual valencies of B cation [42].

Martinez-Ortega et al. explored the effects of partial substitution of La cations in the A site of the lattice of the perovskite structure with Sr cations. Martinez-Ortega et al. explored both La$_{1-x}$Sr$_x$FeO$_{3-y}$ and La$_{1-x}$Sr$_x$CoO$_{3-y}$ perovskite compositions. It was shown that the highest catalytic activity for both compositions was achieved when 20% of the lanthanum was substituted for strontium[42]. In a further study by Batiot-Dupeyrat, et al, explained that this

28

behavior could be explained by the charge compensation effect that can induce the formation of electrophilic oxygen species, such as O^- or O_2^-, which are known to be very reactive toward the C-H bonds or the formation of oxygen vacancies leading to an increase in the oxygen mobility [51]. Additionally, it was discovered that additional strontium substitution resulted in almost constant catalytic activity with a slight decrease in activity as a result decreased in surface area [51]. Additionally, it was observed that the Co-based perovskite samples were fully reducible, whereas the Fe-based perovskite samples were virtually irreducible. It was proven that the Fe-based perovskite successfully oxidized part of the CH_4 into carbon oxides, water, and hydrogen.

2.2.3 Material properties and catalytic activity

Knowledge of the relationship between the catalytic and solid-state properties of inorganic compounds is essential for the systematic design and tailoring of efficient catalysis [48]. A great insight into the material properties and catalytic activity of perovskites comes from research on the oxygen reduction reaction (ORR) for fuel cells and metal-air batteries by Jin Suntivich [52, 53]. Suntivich et al. developed a technique to measure the catalytic activities of oxide catalysts, which is difficult to do due to the poorly defined oxygen transport to and within porous oxide electrodes of several tens of micrometers of thickness. This problem was solved by creating thin films of perovskite oxide particles and bonding them to glassy carbon via an ion-exchanged Nafion binder, and their mass and specific oxygen reduction reaction activities were extracted from rotating disk electrode (RDE) measurements [52]. The RDE is the "workhorse" instrument in electrochemistry and in which the rate of reaction (directly related to current) is measured as a function of potential [35].
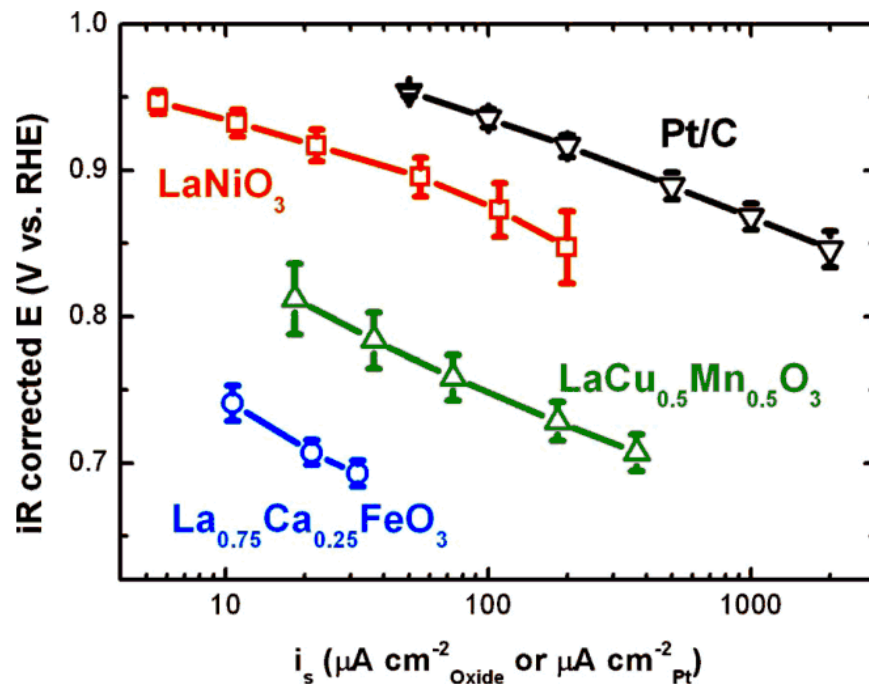
Figure 12. ORR Specific activities i_s and vs. potential after iR and O_2 mass transport correction [52].

Figure 12 shows that $La_{0.75}Ca_{0.25}FeO_3$ has the lowest ORR activity, while $LaNiO_3$ has the higher activity favorable to ORR reduction, which could translate to favorable activity toward combustion. Additionally, compared with the $LaNiO_3$, state-of-the-art platinum nanoparticle catalysts has only an order of magnitude lower specific activity [52].

Using the same methodology, Suntivich et al. investigated a large number of oxides, 15 in total, to establish a catalytic descriptor for ORR [53]. They investigated the hypothesis that the 3d-electron number, which represents the anti-bonding electron occupation of the B-O bond, can influence B-O_2 interaction strength [54].
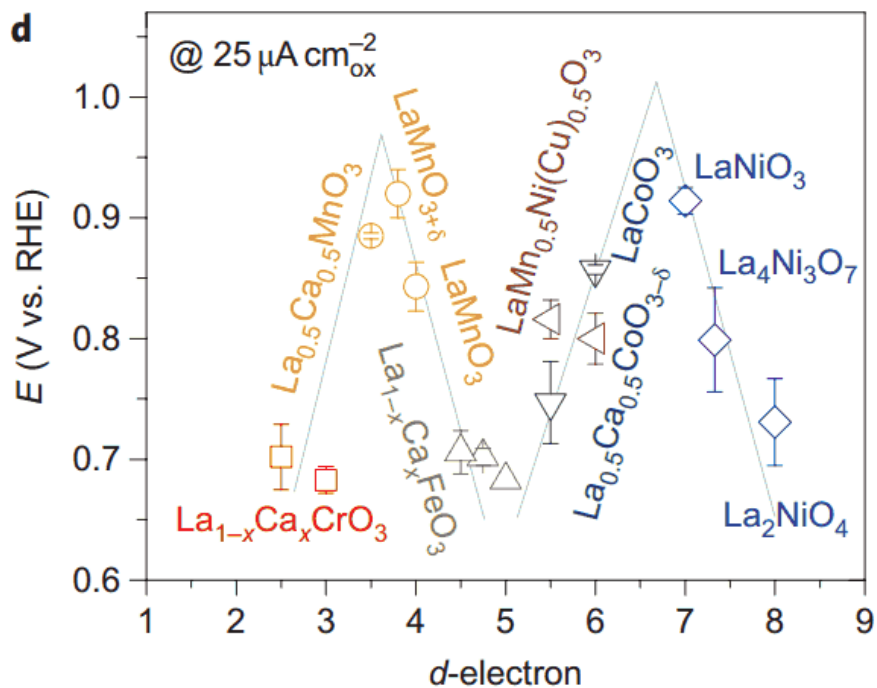
Figure 13. Potential of perovskite oxides. M-shaped relationship with d-electron number.

By plotting the ORR activity of different perovskites vs. their d-electron number per B cation, Figure 13 reveals an M-Shaped relationship with the maximum activity at d^4 and d^7, where the filling of e_g orbital of the transition metal ion located at the surface nears unity. These results suggest that the strength of the B-site transition metal to surface oxygen bond is crucial to efficient catalysis. If the interaction is too weak, or too strong, it would decrease the ORR activity of the given perovskite [55]. Knowledge of this relationship, which links material properties to catalytic activity, allows for accelerating the search for highly active and abundant transition-metal-oxide catalysts to replace platinum on numerous applications, including combustion [53].

2.2.4 Preparation and support

It is relatively simple to synthesize perovskites because of the flexibility of the structure of their diverse chemistry [48]. The perovskite-oxides are generally prepared by citrate, ceramic freeze-drying, co-precipitation, or spray drying. Other preparation methods, such as mist-drying, chelating, and metal-citric-cellulose complexing have been used to increase the final surface area of the catalyst. The surface area of the catalyst is strongly dependent on the preparation method [39].

Perovskites in monolith form have shown to maintain their intrinsic catalytic properties over a wide range of temperatures [39]. It is possible to increase the surface area with water under autogenous pressure at 398-573K or with steam at elevated temperatures. Sintering of bulk perovskite catalysts as a result of high-temperature operation can reduce its surface area [39].

A technique to increase the surface area of the perovskite catalyst is to use it as a thin layer deposited on an appropriate high-surface area support [43]. By dispersing perovskite catalysts in a high-surface area support, it is possible to mitigate the sintering, which reduces the surface-area/active-sites of the structure, of perovskite-oxides at high-temperature operation [39]. The only problem with this approach is the possible solid-state reaction between the precursors of perovskite and its support [43]. The support serves three important functions in a catalyst system [11]:

- It increases the surface area of the active catalysts by providing a matrix that stabilizes the formation of very small particles.
- It increases the thermal stability of these very small particles, thus preventing agglomeration and sintering with consequent loss of active surface.
- In some cases, it provides catalytic activity due to its own special properties.

Batiot-Dupeyrat et al. investigated the effects of $La_{1-x}Sr_xFeO_3$ in methane combustion at a constant temperature of 900°C [51]. In this investigation, it was concluded that the unsupported perovskite-oxides present continuous deactivation with time at a high temperature, mainly due to sintering. In this investigation, the perovskite composition was supported on a $BaAl_{12}O_{19}$ oxide, which is known as thermally very stable, which successfully slowed the deactivation of the catalysts due to sintering.

2.3 Direct conversion of useful thermal output of porous media burners to power

A direct excess enthalpy to power generator is a device that uses excess enthalpy techniques, heat recirculation burners, to create a high-temperature gradient that is utilized to generate power by means of direct energy conversion.

2.3.1 Efficiency

A thermodynamic analysis was done by Weinberg to find the efficiency of energy conversion by thermoelectric devices that operate as part of the heat recycled in regenerative burners [56]. In this analysis, different types of excess enthalpy burners heat exchanger configurations were tested, where some exchangers rejected heat to the cold surroundings or to the incoming reactants as part of the heat recirculation. See Figure 14.
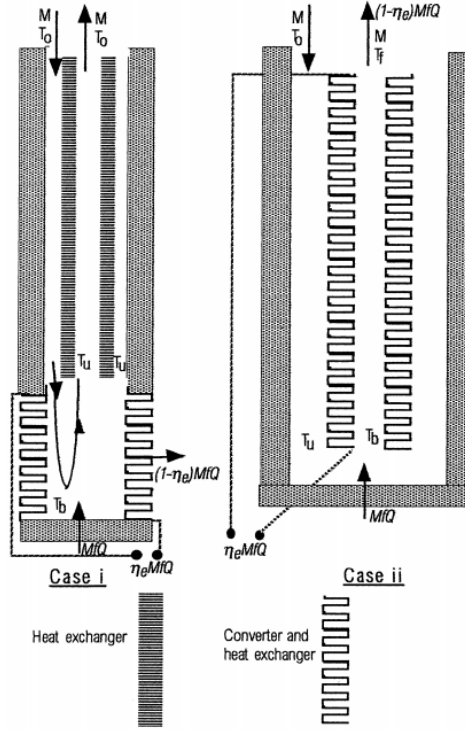
Figure 14. Schematic of two heat exchanger-converter configurations: In case i, the heat is rejected to the surroundings, while in case ii, heat is rejected to the incoming reactants [56].

The efficiency of these burners are bound by the elemental Carnot cycle, where the global efficiency was derived in previous work [57], and are shown for the two seconds in the equation (8).

Efficiency of case i and case ii of Figure 14, where "U" and "L" stand for the upper and lower bounds of the temperature ranges inside of the heat exchangers [56].

$$\eta_i = 1 - \left[T_o/(T_{h,U} - T_{h,L})\right]ln(T_{h,U}/T_{h,L}) \tag{8}$$

$$\eta_{ii} = 1 - \left(T_{c,L}/T_{h,L}\right)$$

Assuming a hypothetically perfect heat exchanger that operates on an infinitesimal temperature difference, surrounded by a converter that uses all the heat of combustion at the maximum temperature and rejects heat to the ambient cold surroundings in addition using temperatures of a reasonable magnitude and using case *i* (which is the better of the two),

34

Weinberg found the maximum thermodynamic theoretical efficiency to be 0.782, while the efficiency of case *ii* was 0.756. In the absence of a heat recirculation technique, the efficiency would drop to 0.604, a 29.5% decrease in overall efficiency from case *i* [56].

2.3.2 Thermoelectric direct energy conversion

In semiconductors and in metals, electrons are free to move while in the conduction band. This movement can be induced by a flux of heat created by a temperature gradient across the metal or semiconductor. This movement of electrons due to heat transfer is analogous to the one created by electric fields in the sense that the motion of electrons transports both their charge and their energy [58]. Thermo electric effects refer to the diffusion of charge carriers, either electrons or holes, in a solid that is exposed to a temperature gradient [59]. This can be taken advantage of by connecting together a n-type and a p-type semiconductor, as seen in Figure 15, and placing them across a temperature difference, thus creating an electromotive force that generates electricity by means of the voltage created across the solid due to the Seebeck effect. This effect occurs when electrons are transported from a region of varying thermal energies, e.g., from the n-type to the p-type semiconductor as they have a discontinuity in the energy levels of the conduction bands [58]. The Seebeck coefficient, S, which is defined as the ratio of the generated electric voltage to the temperature difference and is determined by the scattering rate and the density of the conduction electrons [60].
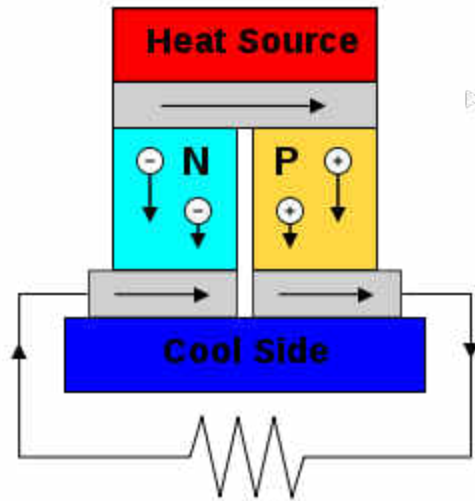
Figure 15. Schematic of a thermoelectric module [59].

The efficiency of a thermoelectric generator is mainly a function of the quality of the temperature difference between the cold and hot side of its junctions and the dimensionless figure of merit (ZT). This figure of merit depends on the materials' Seebeck coefficient (α), electrical conductivity (σ), thermal conductivity (λ), and absolute temperature (T). See equation (9).

$$ZT = \frac{\alpha^2 \sigma}{\lambda} \tag{9}$$

One of the advantages of this type of generator is the scalability; applications that range from personal electronics to fixed power stations can be envisioned [59]. Additionally, thermoelectric generators have a key advantage in their simplicity and reliability due to their lack of moving parts [58].

Now that we have a formulation for the efficiency of an excess enthalpy burner and heat exchanger it is now possible to include the maximum efficiency of a thermoelectric device for the general case of hot and cold temperature, which is expressed as seen in equation (10):

Efficiency of a thermoelectric device

$$\eta_{TEG=}\frac{(T_h-T_c)}{T_h}\ \frac{\sqrt{1+ZT_a}-1}{\sqrt{1+ZT_a}+{}^{T_c}\!/_{T_h}} \tag{10}$$

With this equation, it is now possible to calculate the global efficiency of an excess enthalpy burner, case *i,* by integrating it over the appropriate temperature range, following the same procedure as before for Carnot cycles. Thus, the global efficiency equation from chemical to electric generation becomes, see equation (11):

Total overall efficiency.

$$\eta_{Total} = 1 - \left[T_o/(T_{h,U} - T_{h,L})\right] \int_{T_{h,L}}^{T_{h,U}} \left[\frac{(T_h - T_c)}{T_h}\ \frac{\sqrt{1 + ZT_a} - 1}{\sqrt{1 + ZT_a} + {}^{T_c}\!/_{T_h}}\right] dT_h \tag{11}$$

Thus, the performance of thermoelectric converters that, in rejecting unconverted heat, act as heat exchangers in heat recirculation burners can be considered theoretically. In chase of equation (11), it is evident that the efficiency is mainly a function of the quality of the thermal gradient and the material properties of the thermoelectric materials. Additionally, even though the models in Figure 14 are simple compared with the actual direct excess enthalpy to power generators, they serve as a benchmark as theoretical upper limits to what may be attainable.

2.3.3 Examples of direct excess enthalpy to power generators

Figure 16 shows the experimental schematic of an actual direct excess enthalpy to power generator by Hanamura [61]. In this device, electric power is generated inside thermoelectric porous elements combined with a reciprocating flow flame stabilization technique [32].
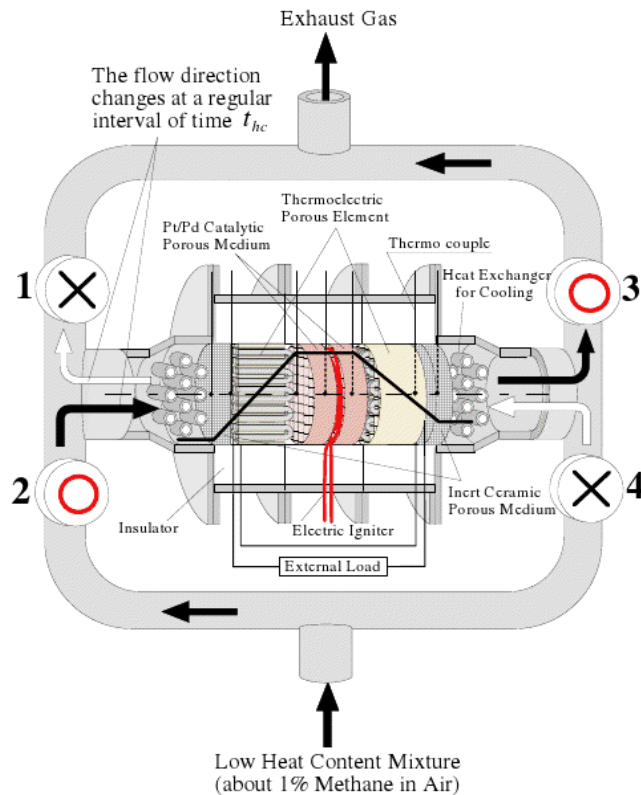
Figure 16. Hanamura experimental setup [61].

Due to the use of combustion in porous media as well as flame stabilization by reciprocating flow, Hanamura achieved super-adiabatic combustion. He also extended the flammable limit to an extremely low equivalence ratio, in essence creating high thermal quality energy, with very low quality chemical energy, in the form of a lean fuel to air mixture. Figure 16 makes it evident that a trapezoidal temperature gradient was created along the flow direction, resulting in a sharp temperature gradient inside the thermoelectric elements. The solid thermoelectric materials of the elements have thermal conductivity of magnitudes higher than

38

gaseous fluids; thus, Hanamura modeled that the configuration of the thermoelectric elements made 94% of the combustion heat to transfer through the elements by means of conduction, in essence, heat rejection to the incoming fluid case *ii* of Figure 14. The total conversion achieved by the device from combustion heat to electric power reached 0.2%; this was done with $FeSi_2$ thermoelectric elements, but it was calculated that, if Ge-Si thermoelectric elements had been used, an energy conversion efficiency of 7 to 10% could be achieved [61].
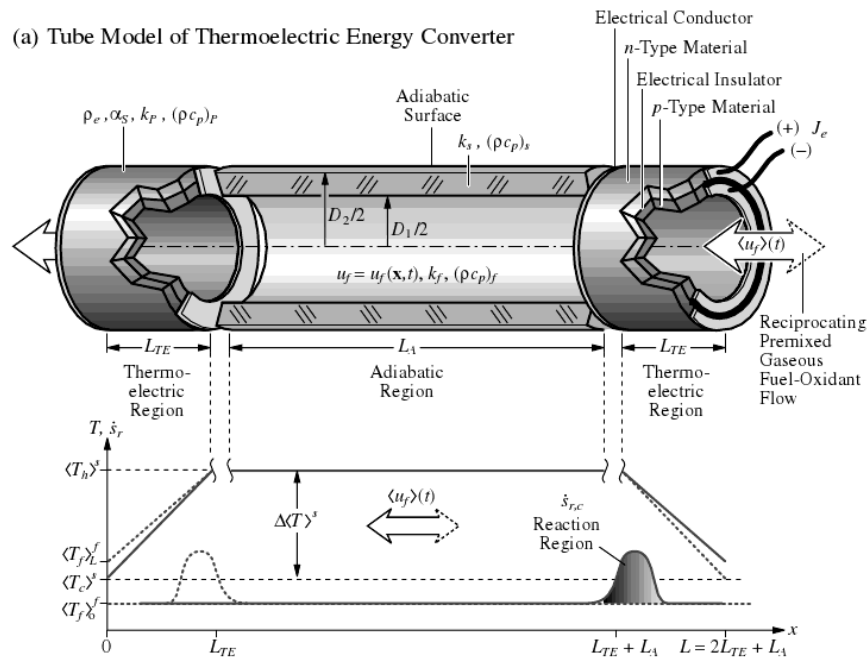
Figure 17. Tube model of thermoelectric energy converter [18].

Figure 17 shows the schematic of another experimental direct excess enthalpy to power generator, in this case by Park [62]. In this experiment, the flame was stabilized with the same reciprocal flow technique and encased in an adiabatic surface in the same way as in Hanamura's experimental setup. However, Park placed the thermoelectric elements to reject heat to the outside environment, case *i* of Figure 14, instead of to the incoming reactants, as in Hanamura's setup. Park used $Si_{0.7}Ge_{0.3}$ thermoelectric elements and achieved an efficiency of 11%. In the

same way as Hanamura, Park argued that if he had better thermoelectric elements, the efficiency could theoretically increase to 25%.
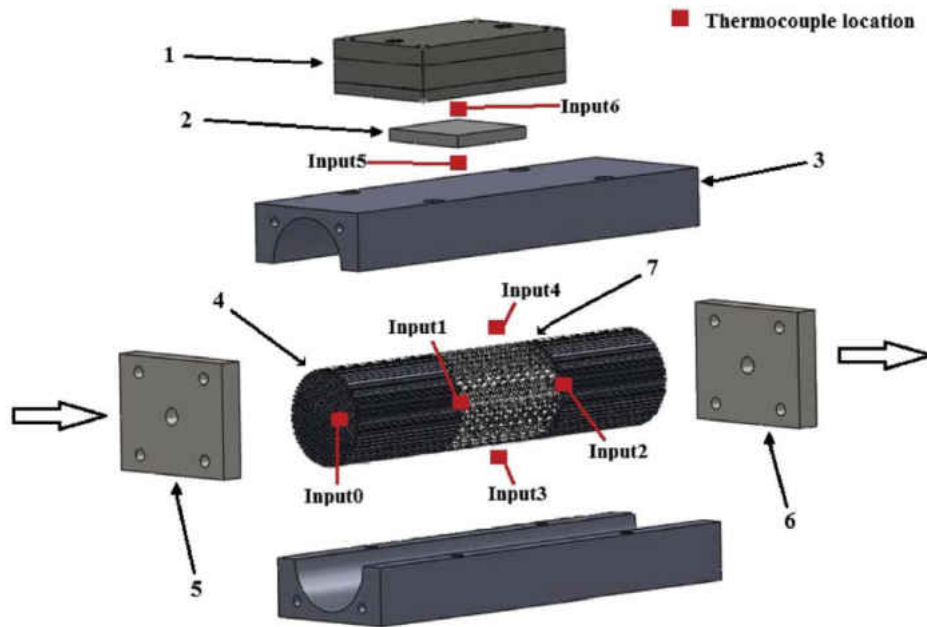
Figure 18. Schematic of porous burner assembly; 1) Air cooling system, 2.) TEG, 3.) Casing, 4.) Low porosity section, 5.) Reactant inlet plate, 6.) Exhaust side plate, 7.) High-porosity section [63].

Mueller et al. explored a way of converting the chemical energy of low-calorific fuels into useful energy, by burning ultra-lean fuel/air mixtures in a matrix-stabilized porous medium combustor [63]. Mueller et al. used a unidirectional burner that used a lower porosity section at both ends of the combustion chamber and a higher porosity section to stabilize the flame, ass seen in Figure 18. The thermal energy was converted into electricity by a thermoelectric module attached at the top of the combustion chamber. In the experiment a combustion chamber featuring an uncoated Al_2O_3 articulated foam achieved a minimum equivalence ratio of 0.589, the device extracted 145 [mW] of energy by means of the thermoelectric device. Similarly, a combustion chamber featuring a SiC coated Al_2O_3 articulated foam achieved a minimum equivalence ratio of 0.634, and extracted 46 [mW] of electrical energy.

CHAPTER 3: DESIGN, MANUFACTURING AND ASSEMBLY

3.1 Configuration design and manufacturing of the combustion chamber

The overall architecture of the combustion chamber is a simple design. The structure itself is just a rectangular prism, as seen in Figure 19. The geometry of the combustion chamber was selected for its simplicity, simplicity that added in the ease of manufacturing of the combustion chamber as well as in its modeling. The 3D modeling and drawings were created using SolidWorks software.
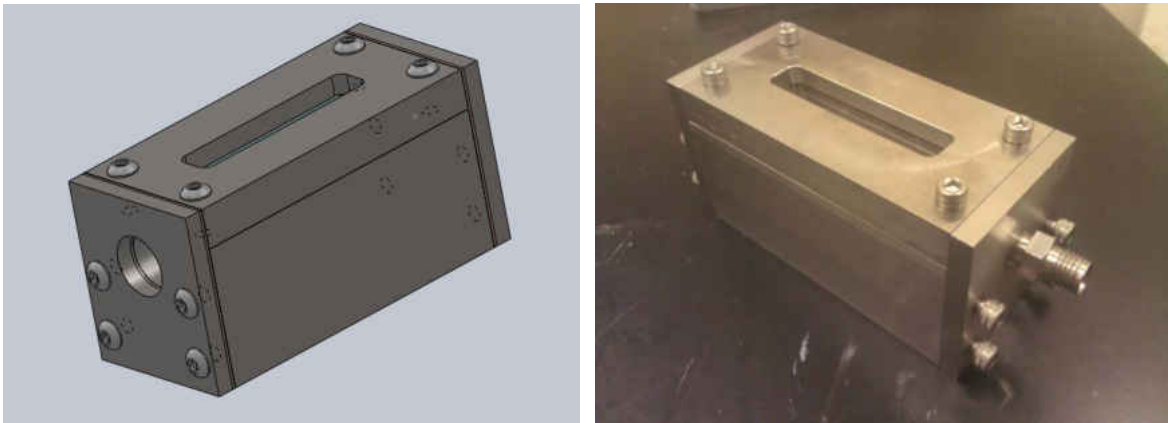
Figure 19: Combustion chamber 3D model and final manufactured assembly.

A rectangular prism, its most important feature is a throughout drilled cylinder tangent to the top surface of the prism, and it has a diameter of 0.75 inches. English units are used in this section to match the drawings, which were made for manufacturing ease in the U.S. The chamber cross section is circular to maximize fluid flow efficiency. During manufacturing, it was important that the diameter was not milled undersized in the manufacturing process. Thus, a bilateral tolerance was utilized for manufacturing purposes were slight over size is preferred. Also eight drill holes with the specifications of a 10-24 size hole with UNC-2B threads were located properly for mounting of end caps. The drawing for the manufacturer is displayed in Figure 20 [64].
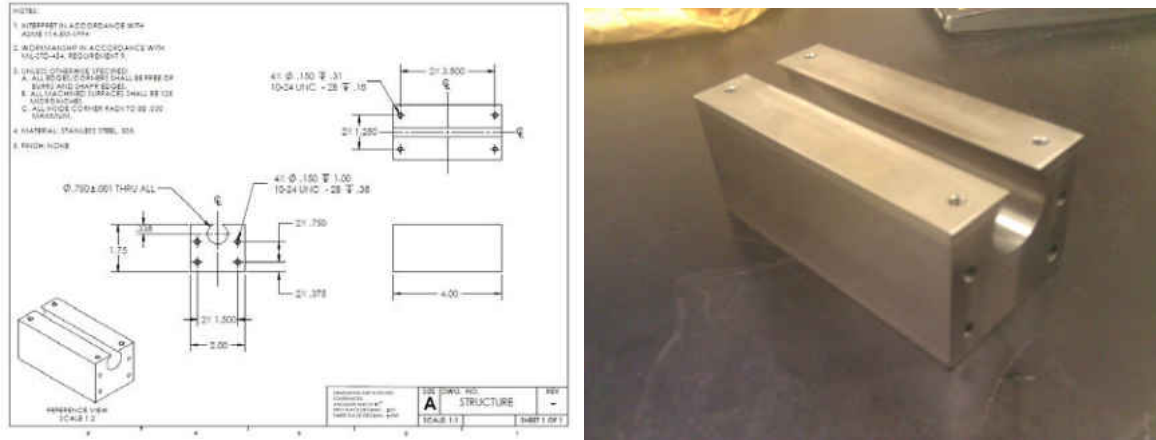
Figure 20: Structure/combustion chamber dimension and tolerances, and final manufactured combustion chamber part.

Tolerances for all parts were defined by two or three decimal places unless otherwise specified. When the dimension is at two places, the tolerance is ±.01. Thus, for more important features, three decimal places for the dimensions are utilized, such as the inlet hole locations. The dimensions of the combustion chamber are 1.75 X 2.00 X 4.00 inches. Stainless steel, grade 303, with no finish was used in the manufacturing of the combustion chamber [64].

The next two items designed were the end caps for the exhaust and gas inlet tubes. These needed to have dimensions similar to the combustion chamber structure. As for mounting the of the end caps, four stainless steel 10-24 screws will be used on each end cap. It is important to dimension the screw hole locations accurately for mating and aligning purposes. Thus, when detailing the drawings for the end caps, the dimensions were called out exactly like the structure to avoid any error. Also being that this was a clearance hole, it was slightly oversized. The drawings for the top and bottom end cap for the assembly and the final machine part can be seen in Figure 20 [64].
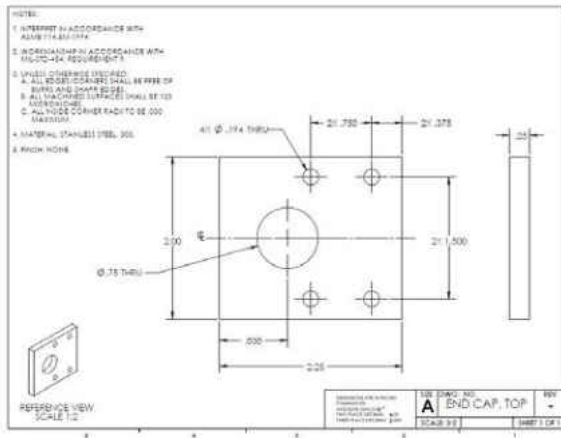
Figure 21: Top end cap dimensions and tolerances.

The most difficult part of the design was to incorporate a window that allowed viewing of the chemical reactions inside the combustion chamber. A quartz glass window compress against the tangent of the chamber was chosen for the design. Due to the high temperatures the combustion chamber is subjected to, a thermal expansion analysis, as well as appropriate tolerance measures, was taken during manufacturing and designs to prevent failure. The drawing for the dimensions and the manufactured quartz glass are displayed in Figure 22 [64].
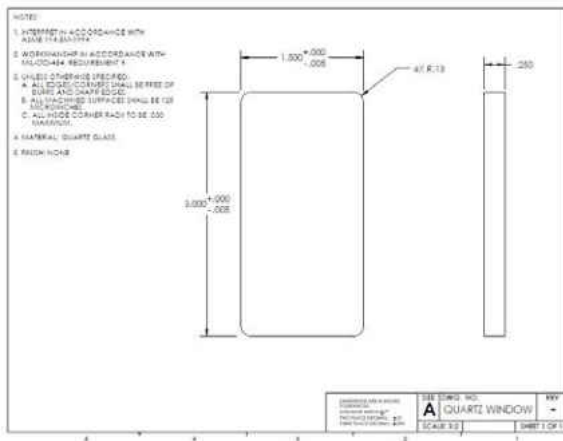
Figure 22: Quartz glass manufacturing drawing and manufactured part.

Note that the bilateral tolerance was used again because the glass will actually fit inside another component. Thus, the glass was designed to be undersized when manufactured. This was done to prevent failure from thermal expansion or compression stress during assembly.

43

The quartz window was designed to be held in place by compression by a stainless steel holder. It would encapsulate the window and hold it in place during run time. The manufacturing drawings, as well as the final manufactured part, can be seen in Figure 23.
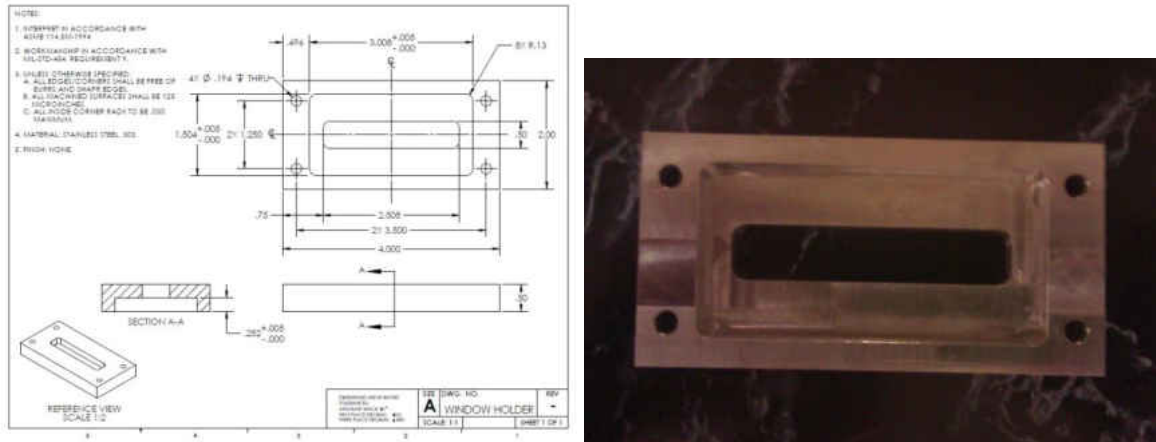
Figure 23: Quartz glass window holder drawing and manufactured part.

The thermal expansion of both the quartz glass and stainless steel part was accounted for in the width, length, and height of where the glass will be assembled. The bilateral tolerance was used again this time where a slight over size is preferred. This configuration is ideal for its purpose because it allows the viewing of the combustion reactions, but will secure the quartz windown with compression for added reliability [64].

Once all the parts were configured to the proper mating dimensions and tolerances, the assembly models and drawings were developed. Assembly drawings are important to prevent assembly errors. With the high level of temperature and gas being burned, it is important that the assembler understands what part goes where and what the actual part is. Thus, in the assembly drawings, a bill of material table is located on the drawing with find numbers. Then each part is ballooned with the corresponding find number and the quantity. The sub-assembly model and drawing of the structure can be referenced in Figure 24 [64].
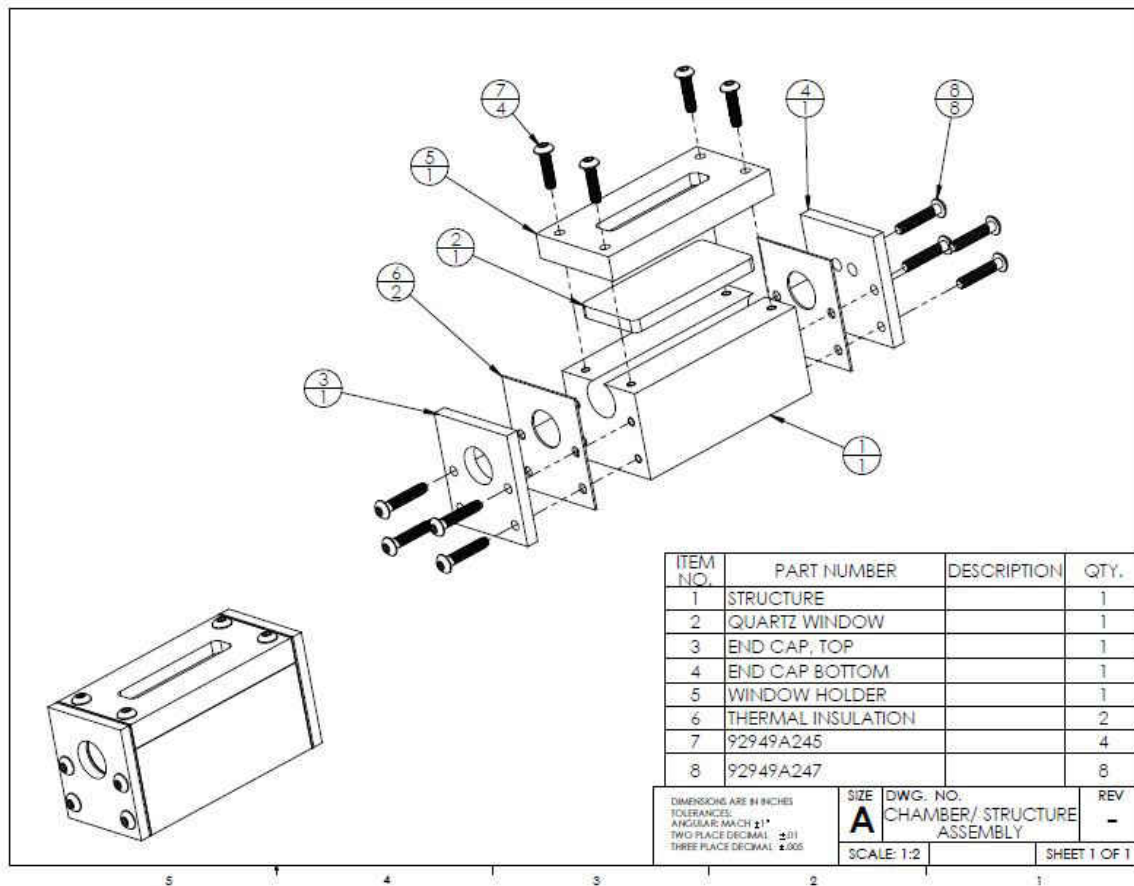
Figure 24: Assembly drawing for structure of the combustion chamber.

Observe the guidelines that were created in both the model and the drawings. This gives a clear view of what order and how to assemble the burner. The final assembly of the combustion chamber can be seen in Figure 19.
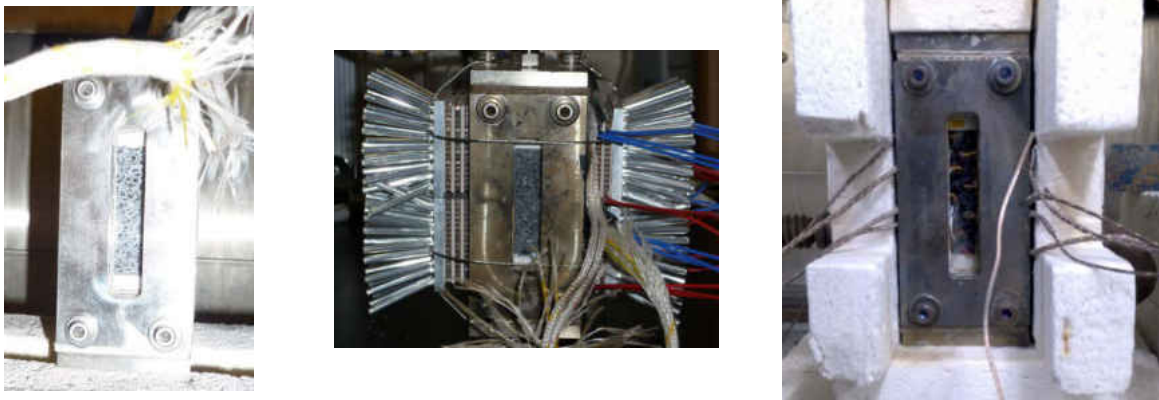
Figure 25: Different experimental setups.

Due to the simplicity of the design, manufacturing, and assembly of the combustion chamber, it could be utilized in a variety of experimental setups. Figure 25 showcases the versatility of the combustion chamber; it shows the assembly of the calibration experiment (left), an experiment incorporating thermo electric generators (center), and a minimum equivalence ratio experiment (right).

CHAPTER 4: EXPERIMENTAL

4.1 Initial testing

The scope of the initial testing of the combustion chamber was to get familiarized its operational parameters. Such as, range of volumetric flow rate, fuel to air mixture ratios, and overall versatility of the device. The device was designed to burn a lean fuel/air mixture using combustion on porous media. The porous media can, in turn, be coated with catalysts or remain uncoated. The heat generated could be harvested by heat engines, such as thermoelectric modules, to generate electricity. Finally, the window allows for diagnostics of combustors and direct observation of the flame.

4.1.1 Preliminary testing of flow range and mixture ratio

The initial testing was done to diagnose the combustion chamber's parametric ranges of operation. Both the tools and the procedures used to acquire data in these tests are crude compared with later experiments. Nonetheless, the data, experience, and skills developed during these experiments were essential for the design and further testing of the combustion chamber.

Figure 26 is a picture of the preliminary testing setup. The air and methane flows were each controlled with Omega (FMA 3200) mass flow controllers. The flow controllers have an uncertainty of ±1.5% of their full-scale range of 0-5 L/min and 0-10 L/min for the methane and air flow meters, respectively. The thermo couples shown in Figure 26 are Omega K-type and are placed to measure the outer steal casing surface temperature. This temperature was of great interest at the time as thermo electric modules were going to be placed in the outer walls of the combustion chamber to harvest the thermal energy as a proof of concept.

Figure 26: Preliminary testing setup.

The first experiment conducted was done to establish the minimum flow rate at which the combustion chamber could sustain a flame, see Table 2. It is a very simple series of experiments where the equivalence ratio is maintained at 1 while the volumetric ratio is decreased. The combustion chamber was ignited at a given flow rate and allowed to reach steady state. A stable, standing, flame was defined in this experiment by observing the flame behavior through the quartz window. A standing stable flame is a flame that does not travel upstream or downstream during a period of time. The minimum mixture flow rate, with an equivalence ratio of 1, was 2.3 liters per minute, see Table 2. It was not possible to achieve a standing wave at lower flow rates.

Table 2: Minimum Flow Rate Experiment [64].

Minimum Flow Rate Experiment (No Insulation)				
AIR [L/min]	FUEL [L/min]	MIXTURE [L/min]	CASING TEMP [C]	EQUIVALENCE RATIO
4	0.416	4.416	410	1
3.8	0.38	4.18	410	1
3.4	0.35	3.75	410	1
3	0.3	3.3	400	1
2.1	0.2	2.3	380	1
Extinguish				

48

The second set of experiments, Table 3 threw Table 5, were designed to find the minimum equivalence ratio that the combustion could achieve at different flow rates. In these experiments, the flow rate was maintained as a constant while the equivalence ratio was reduced. The quartz window was used to diagnose visually whether a flame was stable and standing.

Table 3: Fuel to Air Ratio Experiment at 6 liters per minute air [64].

AIR [L/min]	FUEL [L/min]	MIXTURE [L/min]	CASING TEMP [C]	EQUIVALENCE RATIO	FLAME STATUS
Minimum Fuel to Air Ratio (No Insulation)					
6	0.62	6.62	330	1.00	Stable
6	0.55	6.55	330	0.89	Stable
6	0.5	6.5	350	0.81	Stable
6	0.45	6.45	353	0.73	Stable
6	0.4	6.4	330	0.65	Stable
6	0.39	6.39	330	0.63	Stable
6	0.38	6.38	330	0.61	Extinguished

Table 4: Fuel to Air Ratio Experiment at 8 liters per minute air [64].

AIR [L/min]	FUEL [L/min]	MIXTURE [L/min]	CASING TEMP [C]	EQUIVALENCE RATIO	FLAME STATUS
Minimum Fuel to Air Ratio (No Insulation)					
8	0.83	8.83	440	1.00	Stable
8	0.8	8.8	450	0.96	Stable
8	0.75	8.75	460	0.90	Stable
8	0.7	8.7	475	0.84	Stable
8	0.65	8.65	475	0.78	Stable
8	0.6	8.6	475	0.72	Stable
8	0.55	8.55	475	0.66	Stable
8	0.5	8.5	450	0.60	Stable
8	0.48	8.48	450	0.58	Stable
8	0.46	8.46	450	0.55	Stable
8	0.45	8.45	450	0.54	Stable
8	0.44	8.44	430	0.53	Stable
8	0.43	8.43	430	0.52	Extinguished

Table 5: Fuel to Air Ratio Experiment at 10 liters per minute air [64].

Minimum Fuel to Air Ratio (No Insulation)					
AIR [L/min]	FUEL [L/min]	MIXTURE [L/min]	CASING TEMP [C]	EQUIVALENCE RATIO	FLAME STATUS
10	0.75	10.75	430	0.72	Stable
10	0.7	10.7	450	0.67	Stable
10	0.65	10.65	450	0.62	Stable
10	0.6	10.6	450	0.57	Stable
10	0.58	10.58	450	0.55	Stable
10	0.56	10.56	470	0.53	Stable
10	0.55	10.55	470	0.53	Stable
10	0.54	10.54	450	0.52	Stable
10	0.53	10.53	450	0.51	Extinction

Two important rough conclusions were obtained from these preliminary tests. First, from the data in tables Table 3 threw Table 5, it is evident that the higher the flow rates, the lower the minimum equivalence ratio possible in the combustion chamber. Second, the operational flow range of the combustion chamber is around 2.3 L/min to 10 L/min. Testing of higher flow rates is not possible as the maximum air flow rate for the Omega FMA 3200 flow controller is 10 L/min.

4.1.2 Combustion on porous media coupled with thermoelectric modules proof of concept

The objective of this experiment was to test the coupling of combustion on porous media with a heat engine, in this case thermo electric generators (TEG), as an efficient and elegant means of thermal to electric power conversion. To conduct this experiment, a total of 18 Marlow Industries TG12-6 TEGs were placed in the outer surface of the combustion chamber, see Figure 29. Preliminary testing of these particular TEGs had shown that, for the used form of heating and cooling (passive coupling aluminum heat skinks), a total of three modules per site is the most efficient configuration to generate power, see Figure 27 and Figure 28.
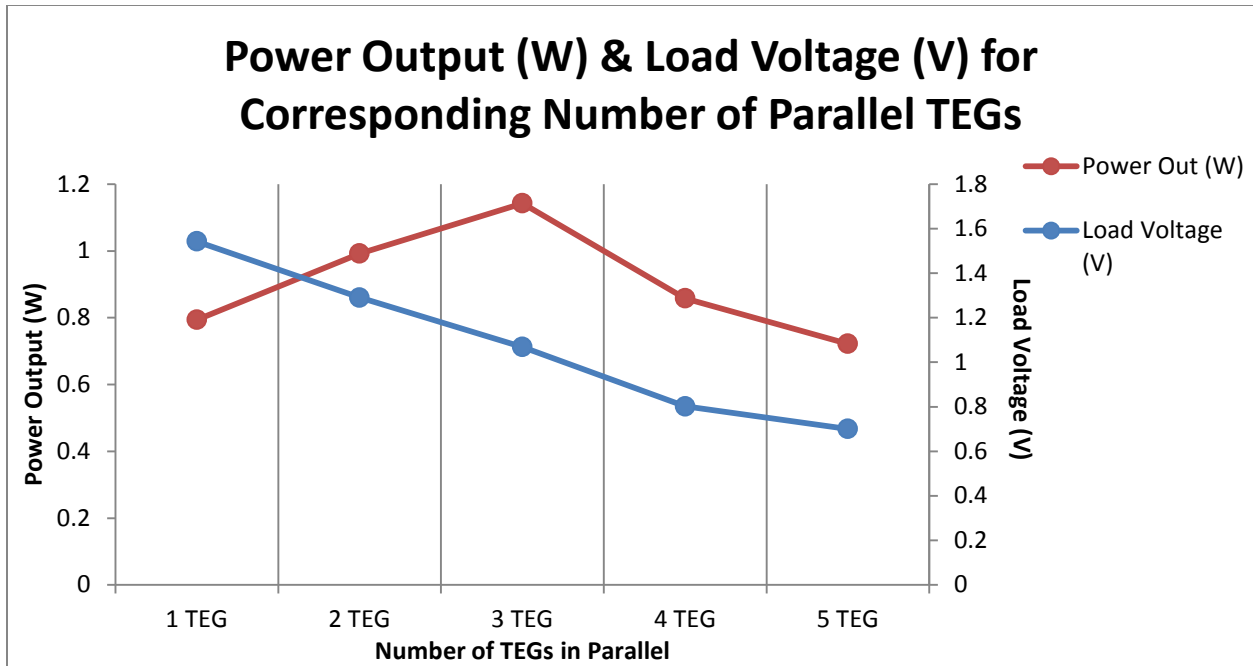
Figure 27: Power output & load voltage for corresponding number of Parallel [65].
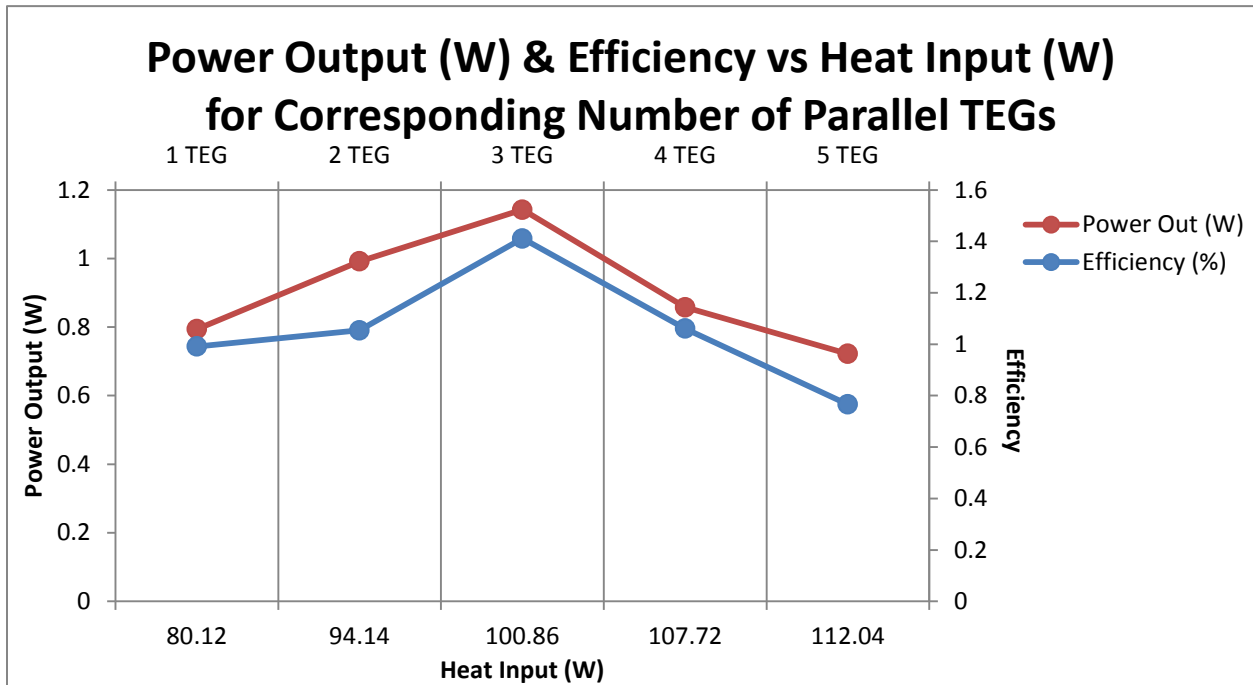
Figure 28: Power output & efficiency vs. heat input to parallel connected module [65].

Figure 29 shows the full assembly of combustion chamber with TEGs; in this picture, 12 of the 18 Marlow Industries TG12-6 TEGs are visible. The quartz window was used to diagnose

the state of the flame. The Omega K-type thermocouples shown were used to monitor the outside temperature of the steel casing as it was necessary to prevent the hot side of the TEGs of reaching their max temperature of 250 °C. The TEGs were connected in parallel and series for an added internal resistance of 5 ohms.

Figure 29: Fully operational assembly of the combustion chamber and TEGs [64].
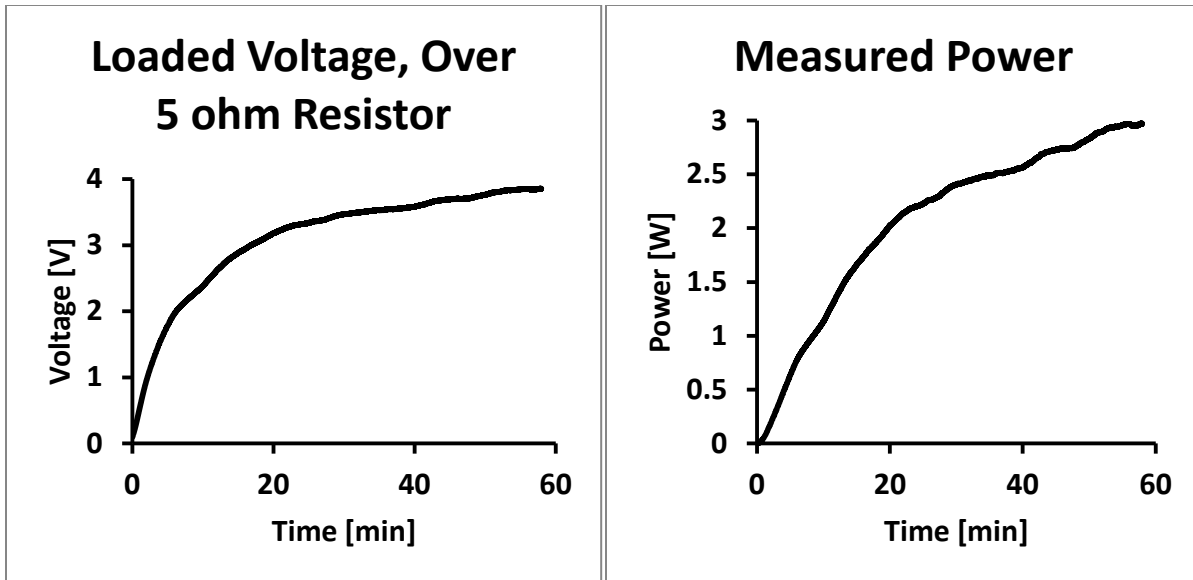
Figure 30: Measured Voltage Output (left) and Measured Power Output (right) [64].

A lean equivalence ratio of 0.56 was picked, and the combustion chamber was allowed to reach steady state. In this experiment, 0.41 L/min of pure methane was mixed with 7 L/min of dry laboratory air to supply the combustion chamber. These flow rates and fuel to air ratios were chosen to minimize the chemical energy input of the fuel while maintaining stable combustion within the media. From this proof of concept experiment, a maximum of 3.2 watts of power was extracted (see Figure 30), which is sufficient power for small electronic devices, such as smart phones. From the total of chemical energy supplied over time by the fuel to the electrical energy generated over time by the TEGs, a total efficiency of 0.176% was calculated.

4.2 Perovskite catalysts enhanced combustion on porous media experiment

<u>4.2.1 Abstract</u>

The effects of La-Sr-Fe-Cr-Ru-based perovskite catalysts on matrix stabilized combustion in a porous ceramic media are explored. Highly porous silicon carbide ceramics are used as a porous media for a catalytically enhanced superadiabatic combustion of a lean mixture

53

of methane and air. The direct observation of the flame during the combustion becomes possible due to a specially designed stainless steel chamber incorporating a quartz window where the initiation and propagation of the combustion reaction/flame was directly visible. Perovskite catalytic enhancement of SiC porous matrix with $La_{0.75}Sr_{0.25}Fe_{0.6}Cr_{0.35}Ru_{0.05}O_3$, $La_{0.75}Sr_{0.25}Fe_{0.6}Cr_{0.4}O_3$, $La_{0.75}Sr_{0.25}Fe_{0.95}Ru_{0.05}O_3$, $La_{0.75}Sr_{0.05}Cr_{0.95}Ru_{0.05}O_3$, and $LaFe_{0.95}Ru_{0.05}O_3$ were used to enhance combustion. The flammability limits of the combustion of methane and air were explored using both inert and catalytically enhanced surfaces of the porous ceramic media. By coating the SiC porous media with perovskite catalysts, it was possible to lower the minimum stable equivalence ratio and achieve more efficient combustion.

4.2.2 Discussion

To extend the lean burning limits using the porous burner, catalysts can be coated on the surfaces of the porous medium. This is particularly advantageous because the porous structure possesses large surface to volume ratio, providing the much needed surface area for applications of heterogeneous catalysts. This study presents the results of coating five different types of perovskite catalysts—$La_{0.75}Sr_{0.25}Fe_{0.6}Cr_{0.35}Ru_{0.05}O_3$, $La_{0.75}Sr_{0.25}Fe_{0.6}Cr_{0.4}O_3$, $La_{0.75}Sr_{0.25}Fe_{0.95}Ru_{0.05}O_3$, $La_{0.75}Sr_{0.05}Cr_{0.95}Ru_{0.05}O_3$, and $LaFe_{0.95}Ru_{0.05}O_3$—to the surface of silicon carbide (SiC) porous structure. The use of such catalytically active materials as a coating for the porous media could have the further benefit of increased flame stability and control of the flame location within of the porous matrix. By employing perovskite catalysts, the activation energy of combustion reactions are reduced, and this lowers the amount of heat recirculated and required for stable combustion within the media. Allowing the flame of a lean mixture to stabilize closer from the inlet of the catalytically enhanced porous structure, at any given flow rate and lean equivalence ratio, this will increase the range of locations where a flame can be

stabilized within the media and, simultaneously, decrease its possible minimum stable equivalence ratio. The equivalence ratio (Φ) is defined as the actual ratio of fuel to oxidant over the ideal ratio of fuel to oxidant where all the fuel has reacted with no excess air, thus being at stoichiometry.

Here the study of superadiabatic combustion of methane inside of the porous matrixes with catalytic enhancement by perovskites is reported. Five different perovskite compositions were used for methane combustion, utilizing different equivalence ratios, and the obtained results were compared to the methane combustion in the SiC porous matrix where no perovskite promoter was present. The lean limit was established depending on the perovskite composition, as well as temperature measurements and determination of the combustion zone locations was performed. The perovskite composition that showed the best results for lean superadiabatic combustions was established.

4.2.3 Experiment design

Figure 31 shows a schematic diagram of the experimental setup used in this work. The combustion chamber is composed of two types of porous media: two alumina honeycomb at each end of the combustion chamber and an articulated SiC or alumina foam in the middle.
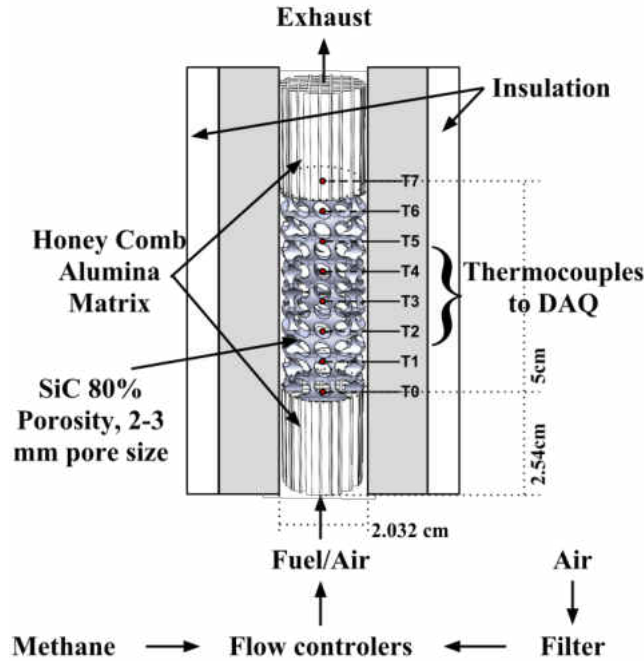
Figure 31. Experimental setup schematic.

The images of the cylindrical articulated foam are shown in Figure 32; the foam is highly porous (85%), has a diameter of 20.32 mm, a length of 50.8 mm, and an average pore size of 2-3 mm. The lower porosity (38%) alumina honeycomb ceramic cylinders that are placed at the inlet and at the exhaust of the combustion chamber, between the reticulated foam, has 8 pores per centimeter, a diameter of 20.32 mm, and a length of 25.4 mm. The average pore size of the honeycomb alumina is much lower than the articulated foam's; this allows the flame to propagate along the axis of the articulated foam ceramic but to be quenched at top surface of the honeycomb. The honeycomb ceramic modules acted as a flame arrestor due to their lower average pore size, forcing the combustion zone to be within the articulated ceramic foam section of the burner.
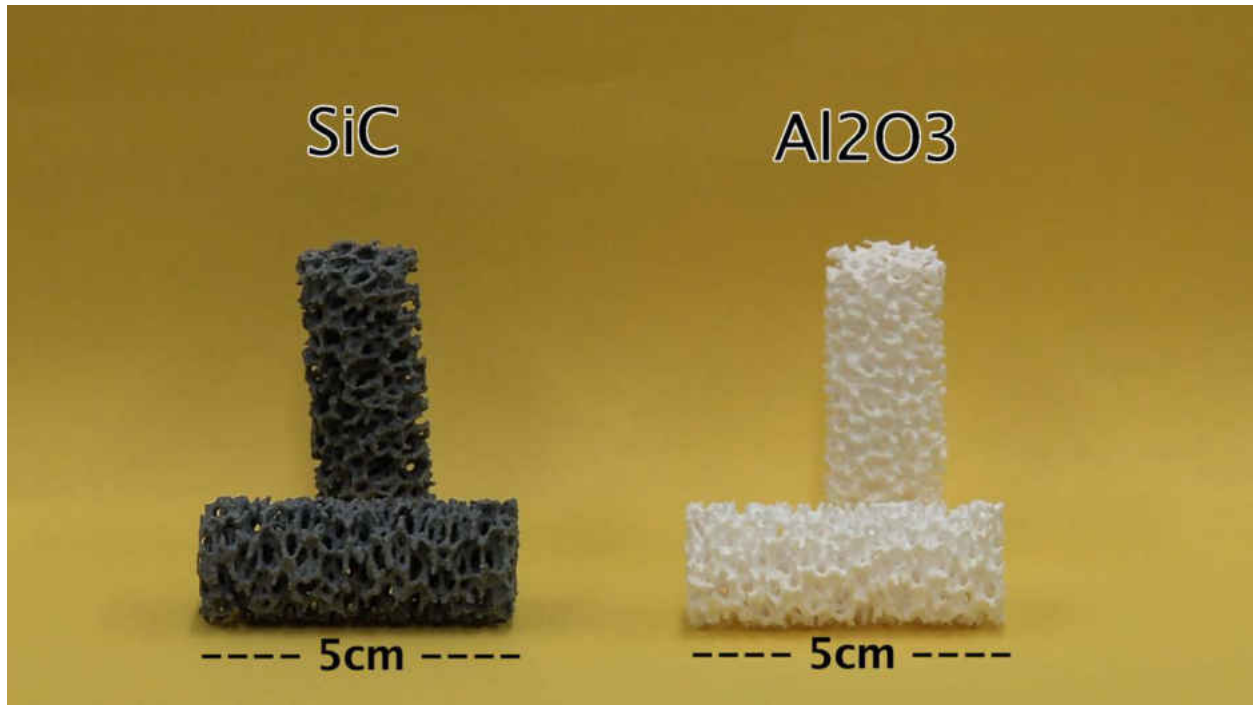
Figure 32. Silicon carbide and alumina articulated ceramic foams used to stabilize the flame inside of the combustion chamber.

Eight K-Type thermocouples were placed along the axis of the cylindrical SiC reticulated foam, equidistantly spaced 7.2 mm apart (see Figure 31), to measure the temperature distribution within the combustion chamber. They have an uncertainty of 0.75%, from 0 to 1250 ^{o}C. The thermocouples were connected to a National Instruments data acquisition system (NI USB-6210) and then logged into the LabView virtual instrument for data collection.

High-grade methane (99% purity) and dry laboratory compressed air were used in the combustion experiment. The mixture of methane and air was formed in a line of sufficient length to allow proper mixing after the two reactant streams meet at a T-junction (Figure 31). The air and methane flows were each controlled with Omega (FMA 3200) mass flow controllers. The flow controllers have an uncertainty of ±1.5% of their full-scale range of 0-5 L/min and 0-10 L/min for the methane and air flow meters, respectively.

The combustion chamber enclosing the porous burner was composed of stainless steel and featured a quartz transparent window that allowed observation of the flame behavior during ignition. In this study, the assembly featured a casing that was insulated on every side with a 25.4 mm thick ceramic fiber board insulation, as seen in Figure 33 (the panel covering the window during combustion experiments is not shown in Figure 33 to better showcase additional details), to reduce heat loss from the burner, to increase the repeatability of the experiments, and to ensure the measurable effects of the catalysts activity in the chemical reactions of combustion.

Figure 33. Porous burner.

Multiple samples of articulated foam ceramics were used in this work. In addition to the uncoated SiC articulated foams, perovskite catalyst $La_{0.75}Sr_{0.25}Fe_{0.6}Cr_{0.35}Ru_{0.05}O_3$, $La_{0.75}Sr_{0.25}Fe_{0.6}Cr_{0.4}O_3$, $La_{0.75}Sr_{0.25}Fe_{0.95}Ru_{0.05}O_3$, $La_{0.75}Sr_{0.05}Cr_{0.95}Ru_{0.05}O_3$, and $LaFe_{0.95}Ru_{0.05}O_3$ coated SiC articulated foams were used inside the porous burner. By conducting several runs of both inert and catalytically enhanced articulated foams the run to run variation and repeatability was measured.

The catalytically active perovskite coatings were deposited on the surface of the porous media using the dip-coating method. Samples of SiC articulated foams were coated with five different compositions of perovskite catalysts. The dip coating process consisted of forming a suspension of the perovskite powders in isopropyl alcohol and placing the slurry mixture in a test tube submerged in a water bath within an ultrasound machine to ensure stability of the suspension. The articulated foam ceramic was then lowered into the slurry and held suspended for one minute, which allowed enough time for the coating to penetrate the pores and bond to the surface. Once coated, the articulated foam was placed in a tray and allowed to dry overnight in the fume hood until all the isopropyl alcohol fully evaporated.

4.2.4 Testing procedure

The reactants were allowed to enter the burner from the bottom of the combustion chamber, as seen in Figure 31. The burner was first ignited using a spark near the top of the articulated foam ceramic or at the thermocouple location T7, at $\Phi = 1.0$. Once ignited, the Φ is reduced to 0.7. At an equivalence ratio of 0.7, the flame is very stable given a cold combustion chamber, and the max temperature of the flame does not exceed 1200 ^{o}C during warm-up. The fuel flow rate was varied to obtain the desired Φ, and the air volumetric flow rate was held constant at 0.008 m^3/min throughout the experiment. After ignition, at $\Phi = 0.7$, the premixed combustion wave propagated in the opposite direction of the flow. Through the quartz window, the combustion zone was observed as a highly luminescent zone slowly traveling upstream. The combustion wave was allowed to travel against the direction of the flow to record the eventual downstream movement of the wave once the Φ is further reduced. This initial value of $\Phi = 0.7$ was used to warm up the combustion chamber. If any of the eight thermocouples reached a

steady-state temperature higher than 1,200 ^{o}C, which as the higher limit of measurement for the thermocouples used in the experiments, the volumetric flow rate of methane was reduced while maintaining the air flow rate constant, reducing Φ. This caused the temperature to drop. The combustion chamber was never allowed to reach temperatures well above 1200 ^{o}C for prolonged periods of time to protect burner components, such as the quartz window and thermocouple wires. Preheating was used as it has a significant effect on combustion on porous media [6]. It was important in this work that the burner was essentially "saturated" with the thermal energy before continuing with the minimum Φ measurement because by such saturation, the effect of catalysts could be accurately accessed.
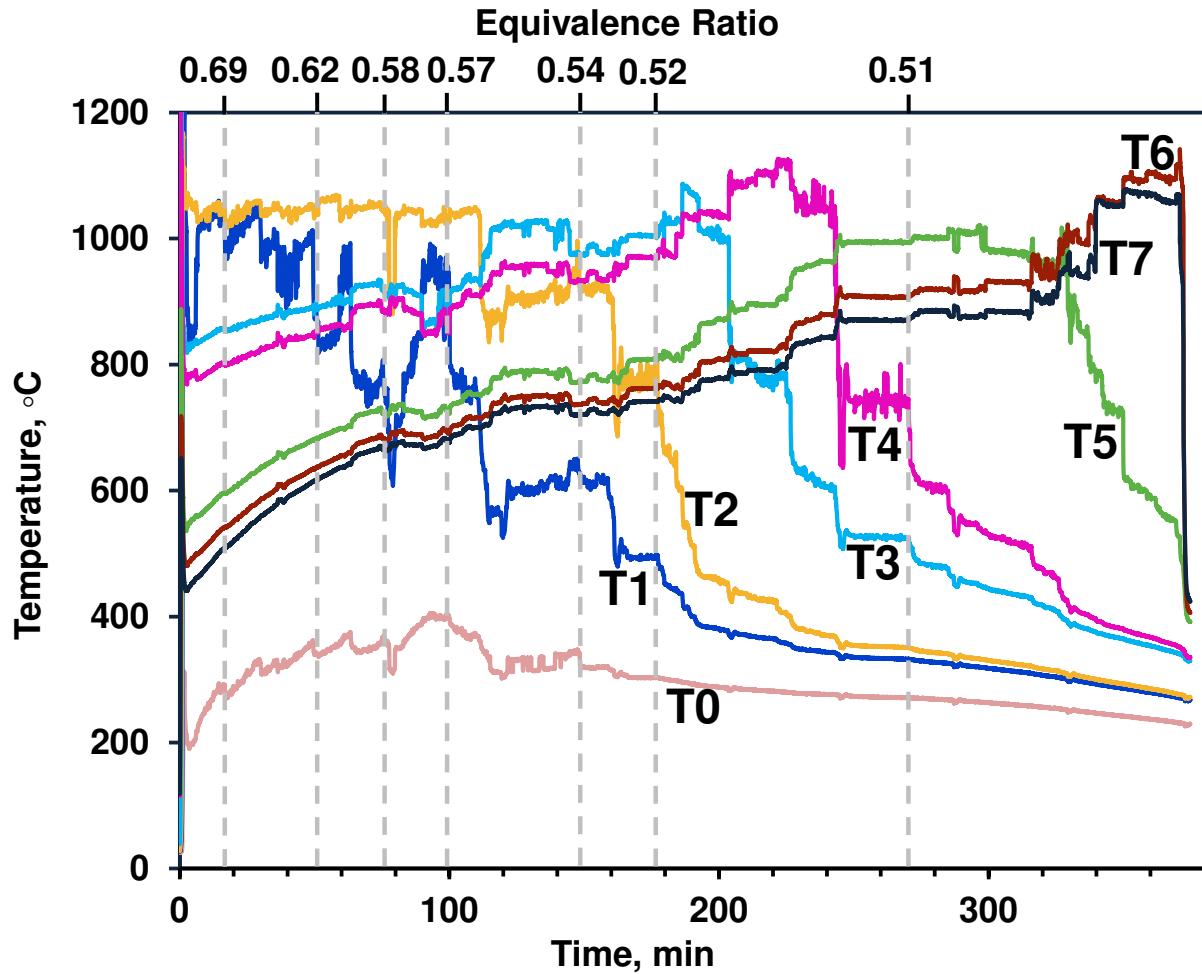
Figure 34. Temperature vs. time of non-coated SiC experiment as the equivalence ratio of the mixture is reduced and steady state temperature profile measurements are taken.

The burner was determined to have reached the steady state if the temperature readings and the flame position had remained steady for 10 minutes. All the temperature data reported here are those measured during the steady state. It is noted that, when discussing the results of Figure 34, this 10-minute criterion was applied whenever the Φ was changed, for example, to reach the condition near the flammability limit. The lean flammability limit was reached at the Φ for which the flame failed to maintain a steady location. The process was repeated for the

articulated foams investigated to document the behavior of the different catalytically enhanced or articulated foam ceramics without perovskite coating.

4.2.5 Results and discussion

By decreasing the Φ in the burner in a step-wise manner, the flame started moving in a step-wise manner downstream. As the flame moved downstream, incoming reactants cooled down the upstream section of the solid ceramic core, increasing the temperature difference between the solid closed to the inlet and the part of the solid downstream from the combustion wave, which enhanced the heat transfer within the solid, thus preheating the reactants. Eventually the heat loss, heat recirculated, and thermal energy generated reached a balance, and the combustion wave slowed to a stop and began to "stand," reaching steady state. As the step-wise downstream movement of the flames neared the end of the solid ceramic length, the radiation to the surroundings becomes a greater portion of the total heat loss [14]. Further, decreases in Φ will eventually cause the flame to blow off or exit the SiC articulated foam and to be extinguished. The feedback of heat transfer from products to the reactants is, in part, a function of the porous media thickness and the position of the flame within the media with respect to the media's inlet and outlet [4, 14, 20].

Figure 34 shows the typical time trace of temperature collected from the experiments using SiC porous media. During the preheating stage of the experiments, the flame propagated upstream and began to stand near thermocouple location T2, as seen at minute 0 in Figure 34. Once steady state was reached, or the temperature approached 1,200 $^\circ$C, the amount of methane in the mixture was reduced. The Φ was reduced at minute t = 19, t = 45, t = 78, t = 100, t = 145, t = 178, and t = 265, shown by the dash lines in Figure 34. The decrease in Φ would result in less

heat generated to heat up the incoming fuel-air mixture, and therefore, there would be insufficient heat to sustain a stable combustion at a fixed position [6]. The combustion wave retreated to a downstream location until a balance between heat generation, increased heat recirculation, and heat loss was reestablished to stabilize the flame to stand again. This process is observed between the time intervals of t = 0-19, t = 45-78, t = 78-100, t = 100-145, t = 145-178, and t = 178-265 minutes in Figure 34. The drop in temperature at the thermocouple location with the highest temperature after the dashed line and the increase in temperature of the next thermocouple location after the dash line in Figure 34 demonstrate how the combustion wave moved downstream as the Φ was reduced. For example, the temperature peak detected by thermocouple T4 occurred around t = 220 minutes, while that for T3 is around t = 190 minutes. One might conclude that as the Φ is reduced, the flame location moves in the downstream direction. Such downstream movement of the combustion wave due to lowering of the Φ is more apparent in Figure 35.
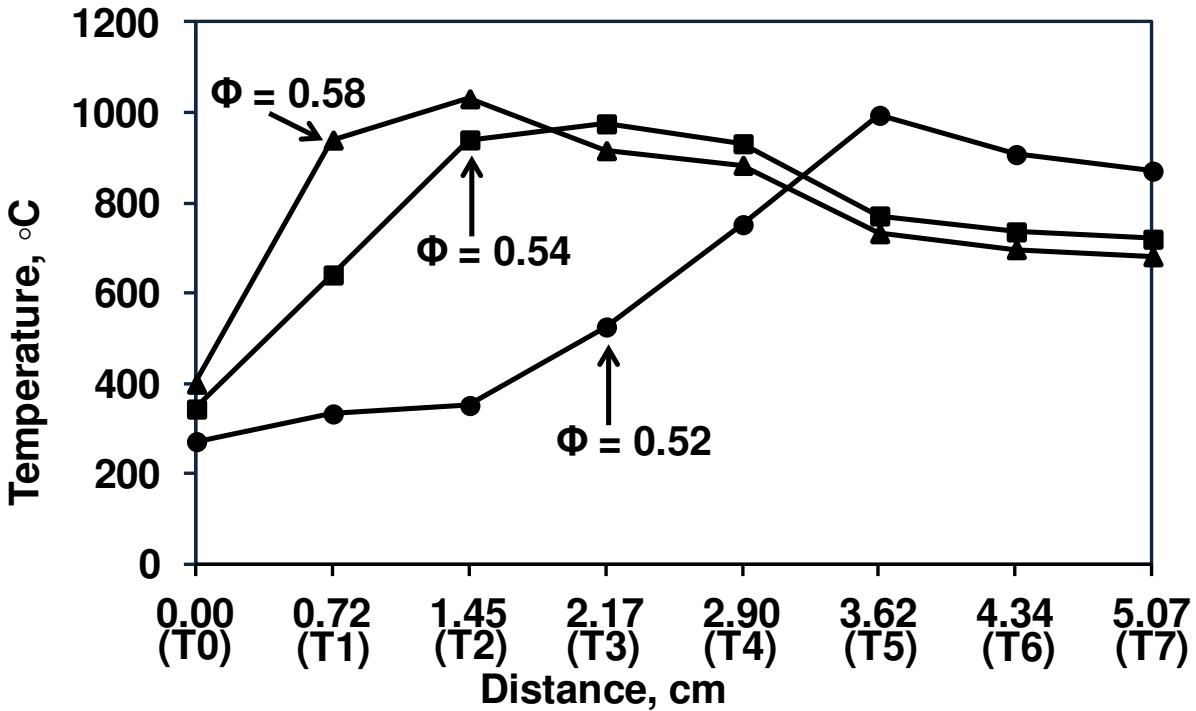
Figure 35. Shows the temperature of the thermocouple locations versus axial distance, along the axis of the combustion chamber, of the stabilized standing combustion wave at 0.58, 0.54, and 0.52 equivalence ratios.

Where it is shown that the flame moves and stabilizes at a downstream location once the equivalent ratio is reduced, the temperature profiles shown are taken when the burner has reached steady state and when the flame has begun to stand. Additionally, the magnitude of the flame displacement due to the change in Φ becomes apparent. The temperature distribution at $\Phi = 0.58$, taken at $t = 98$ minutes, shows that the flame stabilized at the thermocouple location T2 with a maximum temperature of 1,030 ^{o}C. At $\Phi = 0.54$, the flame has propagated downstream from thermocouple location T2 and has begun to stand at thermocouple location T3 with a maximum temperature of 975 ^{o}C. At $\Phi = 0.52$, the flame stabilized at thermocouple location T5 with a maximum temperature of 994.3 ^{o}C. The flame moved downstream from the thermocouple location T2 to T5 as Φ was reduced from 0.58 to 0.52. Such controlled location of the flame inside of the porous media as a function of equivalence ratio is important because it allowed the

flame to stabilize in a controlled manner, thus increasing the homogeneity of temperature distribution, increasing the range of volumetric flow rates that the burner can support, and allowing more efficient combustion.
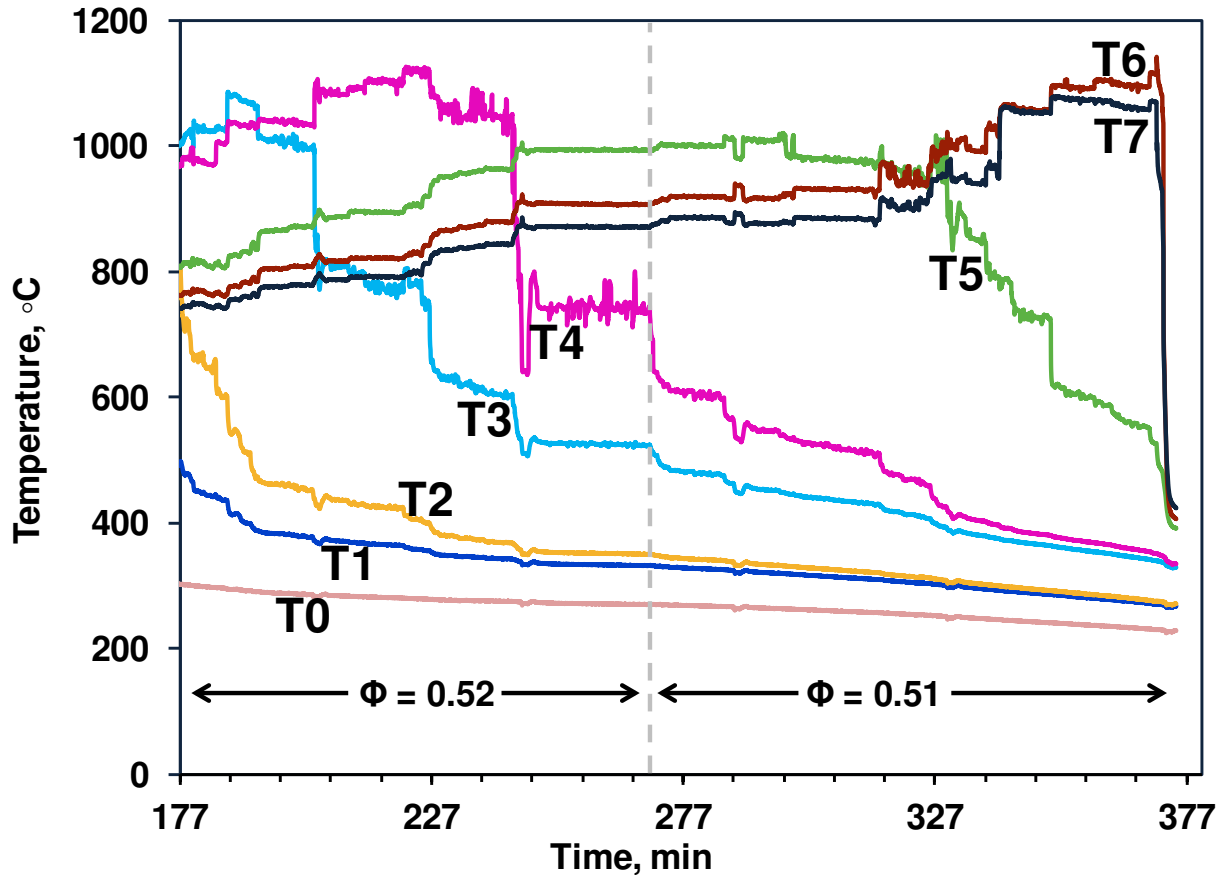
Figure 36. Temperature vs. time of non-coated SiC at lowest equivalent ratio, minimum stable equivalence ratio happen between min 250-270.

Figure 36 shows the data with higher resolution from the same run as Figure 34 for t = 177-377 minutes, a shorter time range toward the end of the experiment. At t = 177 minutes, the wave is stabilized at thermocouple location T3, with a T_{max} = 1,004 ^{o}C. After the Φ has been reduced, the temperature at that location drops at t = 185 minutes, followed by an increase at thermocouple location T4 from T = 976 to T = 1099. This is due to the downstream motion of the combustion wave. Eventually, the downstream displacement motion of the combustion wave

slows down and begins to stand, starting at 250 minutes, the temperature profile around minute 260 is the location of the temperature profile (Φ = 52) in Figure 35. Additionally, it is evident that after reducing the Φ again at minute 270 of Figure 36, the downstream motion of the wave continues to thermocouple location T6 and T7 until it is quenched by the lower porosity honey comb alumina ceramic. Thus, the temperature profile at minute 260 of Figure 36 and the line labeled (Φ = 52) in Figure 35 are at the lowest stabilized Φ where the combustion chamber can sustain a standing wave.

Table 6. Inert and Peroviskite coated SiC tabulated results

Coating Composition of SiC Articulated Foam	T_{max} at Φ=0.58, °C	T_{max} at Minimum Stable Φ, °C	Minimum Stable Φ	Number of Runs
Un-Coated (Inert)	1030.9	994.3	0.547±0.018	4
$La_{0.75}Sr_{0.25}Fe_{0.60}Cr_{0.35}Ru_{0.05}O_3$	1158.5	1081.4	0.525±0.021	2
$La_{0.75}Sr_{0.25}Fe_{0.60}Cr_{0.40}O_3$	989.4	1056.2	0.525±0.007	2
$La_{0.75}Sr_{0.25}Cr_{0.95}Ru_{0.05}O_3$	953.9	1041.5	0.535±0.007	2
$LaFe_{0.95}Ru_{0.05}O_3$	1033.7	1072.9	0.53	1
$La_{0.75}Sr_{0.25}Fe_{0.95}Ru_{0.05}O_3$	906.6	1039.2	0.51±0.01	3

Multiple experiments were done to collect data for inert SiC articulated porous media and catalytically enhanced SiC. Table 6 shows the tabulated results, specifically the minimum stable Φ achieved, for inert uncoated SiC articulated ceramic foam and for the SiC catalytically enhanced with five different compositions of perovskite catalysts: $La_{0.75}Sr_{0.25}Fe_{0.60}Cr_{0.35}Ru_{0.05}O_3$, $La_{0.75}Sr_{0.25}Fe_{0.60}Cr_{0.40}O_3$, $La_{0.75}Sr_{0.25}Cr_{0.95}Ru_{0.05}O_3$, $LaFe_{0.95}Ru_{0.05}O_3$, and

$La_{0.75}Sr_{0.25}Fe_{0.95}Ru_{0.05}O_3$. The ± sign in the table shows the standard deviation, or run-to-run variation, between the results of the multiple runs with the same configuration of coated or uncoated articulated foam ceramics. These prove that all five different perovskite compositions yielded better results at lowering the minimum stable Φ compared with the uncoated SiC articulated foam.

The trend of lowering Φ by doping mixed ionic electronic conducting perovskites can be observed from the results presented in Table 1. While all perovskite-coated porous media show improvement for lowering the Φ in comparison with uncoated SiC foam, the best results were achieved for perovskite composition where both Cr^{3+} ions and Fe^{3+} ions were present in addition to the existence of minute quantities of Ru^{3+}/Ru^{4+} ions. It is known that Cr^{3+} ions in ABO_3 perovskite structure create rather stable and non-catalytically active ceramics, which can be well used as interconnect in solid oxide fuel cells [66] due to its stability in oxidizing and reducing environment and high electronic conductivity [67]. Therefore, three compositions $La_{0.75}Sr_{0.25}Cr_{0.95}Ru_{0.05}O_3$, $La_{0.75}Sr_{0.25}Fe_{0.60}Cr_{0.35}Ru_{0.05}O_3$, and $La_{0.75}Sr_{0.25}Fe_{0.60}Cr_{0.40}O_3$ used in the present experiment did not show the best catalytic enhancement of combustion. However, despite the presence of non-active Cr^{3+} ions, the availability of catalytically active Fe^{3+} ions in the perovskite lattice slightly improved the performance of $La_{0.75}Sr_{0.25}Fe_{0.60}Cr_{0.35}Ru_{0.05}O_3$ and $La_{0.75}Sr_{0.25}Fe_{0.60}Cr_{0.40}O_3$ even when Cr^{3+} ions were also present. The composition $LaFe_{0.95}Ru_{0.05}O_3$ did not show the best results even though the Cr^{3+} ions were not present. This can be explained by the fact that the A site of ABO_3 perovskite is presented by La^{3+} ion without any substitution of La^{3+} with Sr^{2+}, which leads to almost stoichiometric quantities of O^{2-} ions and decreases the amount of oxygen vacancies in the lattice. As a result, both ionic and electronic conductivities, along with oxygen mobility and catalytic activity of $LaFe_{0.95}Ru_{0.05}O_3$ perovskite,

are decreased in comparison with compositions where a certain quantity of La^{3+} ions are substituted with Sr^{2+} ions in the lattice. The $La_{0.75}Sr_{0.25}Fe_{0.95}Ru_{0.05}O_3$ perovskite showed the most promising catalytic activity toward enhancement of superadiabatic combustion as it has both La^{3+} ions substituted with Sr^{2+} ions; Cr^{3+} ions are absent on B site of the perovskite lattice and, at the same time, a small number of Fe^{3+} ions were substituted with very active Ru^{3+}/Ru^{4+} ions, bringing the best performance in catalytic enhancement of combustion.
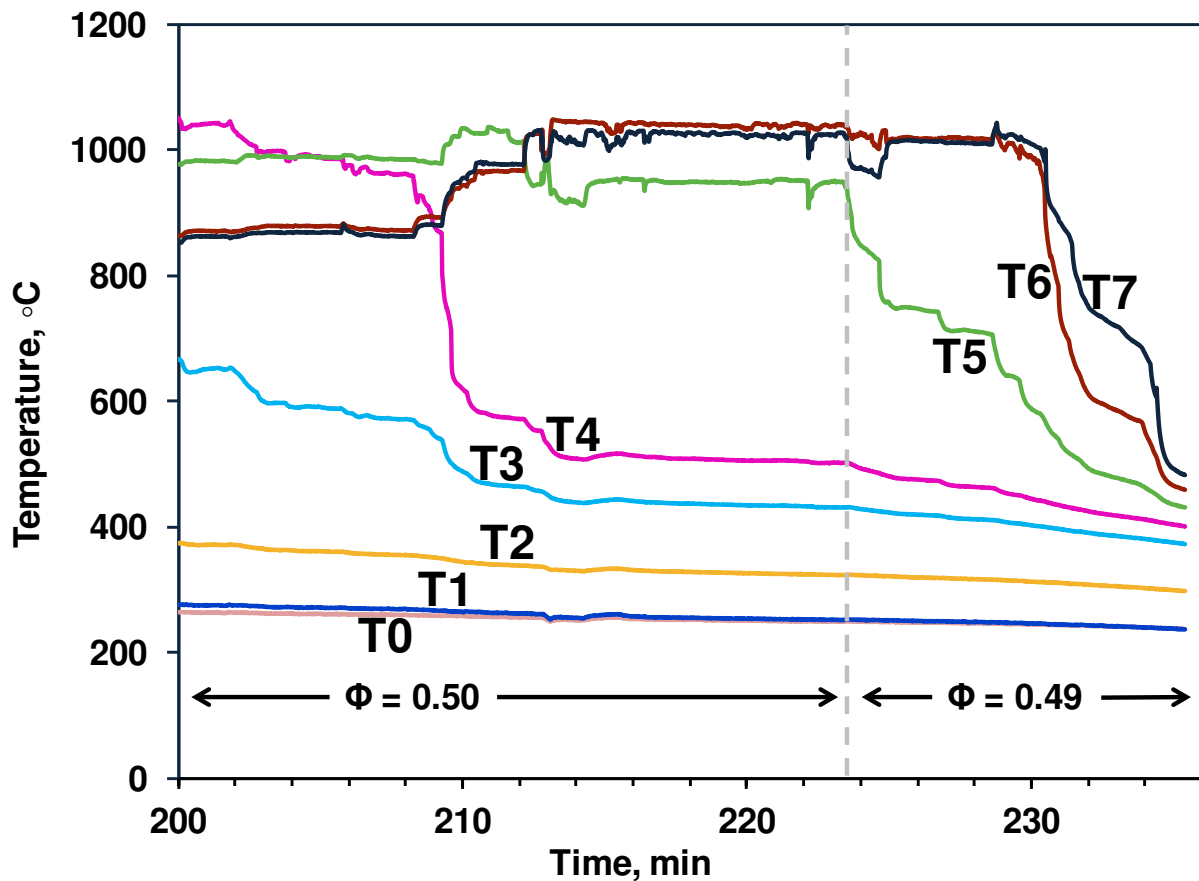
Figure 37. Temperature vs. time of La0.75Sr0.25Fe0.95Ru0.05O3 coated SiC at lowest equivalent ratio, minimum stable equivalence ratio happen between min 215-223.

Figure 37 shows the last minutes of a run with the SiC porous combustion chamber enhanced with $La_{0.75}Sr_{0.25}Fe_{0.95}Ru_{0.05}O_3$. The data was collected with the same procedure as the data collected for the uncoated SiC foam run(s) shown in Figure 34, as well as all the SiC foams

coated with the five different types of perovskites. The flame was successfully stabilized for $\Phi =$ 0.5 at the thermocouple location T6 with a T_{max} of 1039 ^{o}C. The minimum average Φ achieved by an inert SiC articulated foams was 0.547 while the catalytically enhanced SiC porous media reduced the minimum stable Φ to 0.535-0.51; $La_{0.75}Sr_{0.25}Fe_{0.95}Ru_{0.05}O_3$ perovskite provided the best results with a minimum average Φ of 0.51.
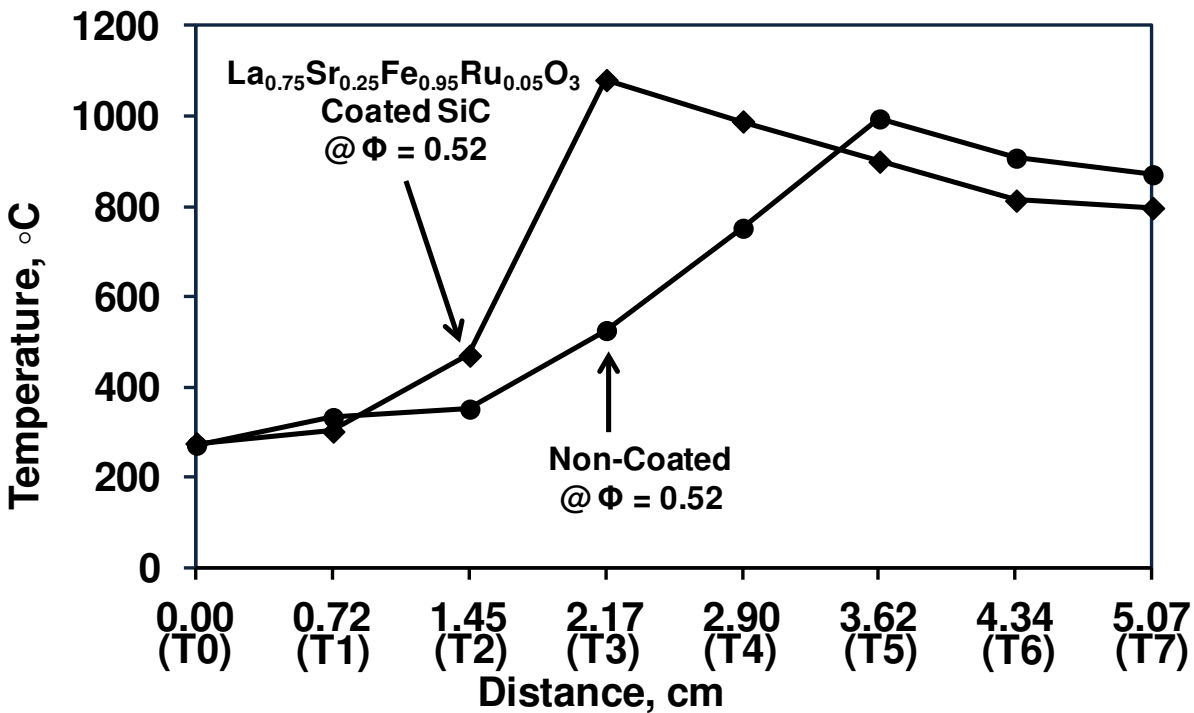
Figure 38. Temperature gradient comparison between coated and non-coated SiC at the same equivalence ratio.

Figure 38 shows another feature of the perovskite catalytic enhancement in combustion in porous media. It shows the temperature distribution of non-coated SiC compared with the catalytically $La_{0.75}Sr_{0.25}Fe_{0.95}Ru_{0.05}O_3$ enhanced SiC at a matching Φ of 0.52. The perovskite-coated SiC stabilized at the thermocouple location T3, with a T_{max} of 1072 ^{o}C, while the non-coated SiC stabilized at the thermocouple location T5, with a T_{max} of 994 ^{o}C. It is a total of 1.45

cm of displacement difference of the flame location, while having both the same Φ and volumetric flow rate.
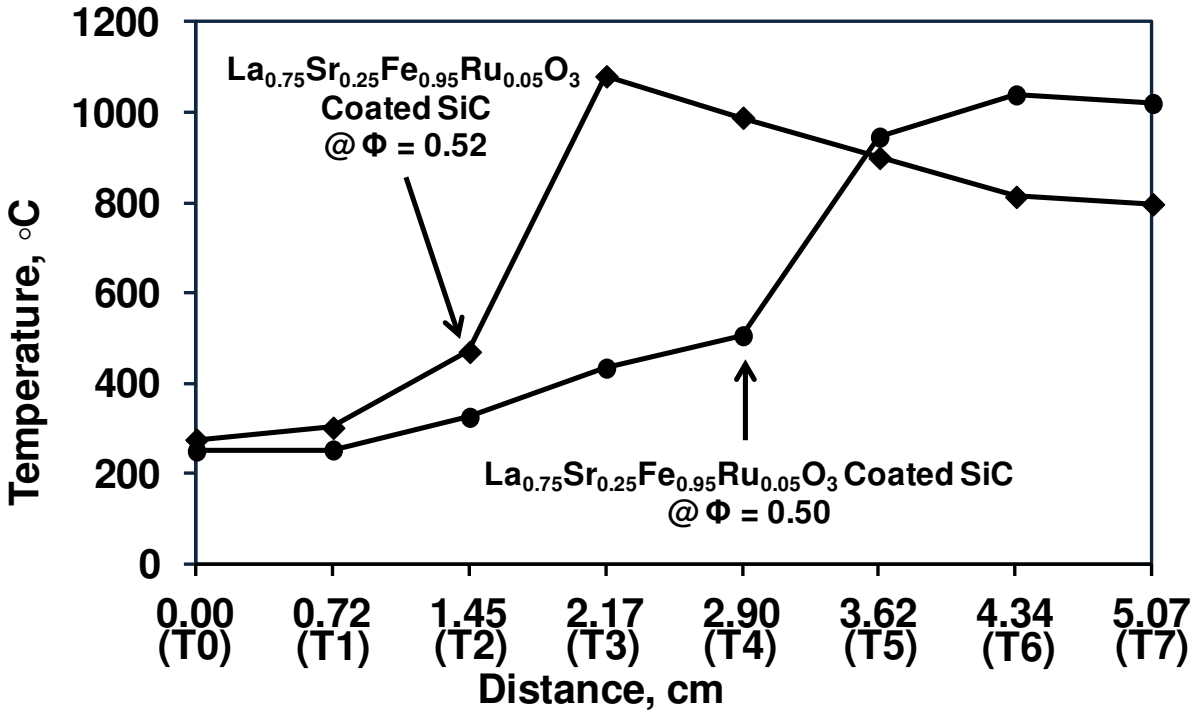
Figure 39. Temperature gradient as a function of equivalence ratio of a La0.75Sr0.25Fe0.95Ru0.05O3 coated SiC at different equivalent ratios.

Figure 39 shows the temperature distribution of the enhanced SiC with $La_{0.75}Sr_{0.25}Fe_{0.95}Ru_{0.05}O_3$ at a stabilized standing wave with an Φ of 0.52 and 0.50. The minimum stable Φ was 0.5, which the flame stabilized to a standing wave located at T6 while at $\Phi = 0.52$, the flame successfully stabilized at T3. Thus, by examining results of Figure 38 and Figure 39, it is evident that by coating the porous SiC articulated foam with perovskite catalysts, the combustion wave can stabilize closer to the inlet at any given Φ, in the same way an increase in Φ (as seen in Figure 35) or lowering of the flow rate [14] can help stabilize the flame upstream. For the flame to stabilize at a given position in the porous media, the right balance of chemical input, thermal energy recirculation, and heat loss must occur. By enhancing the surface area of

the porous media with high-temperature perovskite catalysts, the activation energy required to release the chemical energy of the reactants is reduced. It effectively increases the minimum stable Φ that a catalyzed porous burner can achieve.

CHAPTER 5: CONCLUSION

"Where there's muck there's brass" is a 20th century expression originated in Yorkshire, England, where brass was used as a term for money and where the fires of the industrial revolution were burning hot and rich, spewing a significant amount of soot into the air. Today, thanks to advances in technology, we can still relate energy generation to wealth but not as much "muck." The reason for this is that due to a better understanding of combustion, it has been possible to decrease the amount of pollution while increasing the amount of useful thermal energy that can be extracted from fuel. Nonetheless, the combustion techniques used today are not perfect, and there is still significant work needed to fulfill the environmental and energy demands of tomorrow.

In this work, a combustion chamber was designed incorporating two advance combustion techniques: combustion in matrix stabilized porous media (CMSP), and perovsikite catalytically enhanced combustion (PCEC). These techniques were coupled with a simple heat engine, thermoelectric modules, to generate power and act as proof of concept for a portable heat and power device. Both combustion techniques, CMSP and PCEC, increased the rate of reaction in combustion, which follows the Arrhenius type relationship: $\exp(-E_a/RT)$. Combustion in porous media increases reaction rates by increasing the maximum temperature, T, achieved at a given ratio or concentration of fuel and oxidant, while catalytically enhanced combustion increases combustion rates by giving alternative reaction pathways to heterogeneous combustion, realizing radicals directly decreasing the activation energy, E_a, needed to initiate the reaction.

The combustion chamber was designed with simple geometry and careful selection of materials. The simple geometry was selected to ease manufacturing and to help with model verification. Various experiments were designed to test and calibrate the combustion chamber.

Matrix stabilized combustion on porous media was successfully performed. When coupled with thermoelectric devices, the heat and power unit generated enough electricity to power a small electronic device.

Various perovskite compositions were deposited on the surface of the SiC articulated foam used to stabilize the flame in the combustion chamber. The performance of these compositions during combustion was tested. The mixed ionic electronic conducting perovskite compositions proved adequate catalysts to lower the minimum equivalence ratio possible in the combustion chamber. These results indicated that by coating the articulated foams with perovskite-type catalysts, the reaction rate of combustion was increased. The best perovskite composition tested was $La_{0.75}Sr_{0.25}Fe_{0.95}Ru_{0.05}O_3$, which reduced the average minimum equivalence ratio to 0.51 ± 0.01 from 0.547 ± 0.018 when compared with tests of non-perovskite coated inert experiments.

To solve the problems of burning low-calorific fuel for heat, energy, or both, combustion on porous media coupled with perovskite catalytically enhanced combustion is an elegant solution. Both techniques increase the reaction rates of lean combustion, and due to their mechanics, they complement each other. The high surface area of the articulated ceramics used in porous media acts as the perfect support for catalysts. Additionally, the increase in local maximum temperature of a given mixture created by the heat recirculation in combustion in porous media increases the thermodynamic efficiency of the energy that can be extracted from a combustion chamber by a heat engine. Finally, it was demonstrated that due to the decrease in activation energy from catalytic enhancement, the minimum equivalence ratio that could be sustained in the combustion chamber was decreased. This can translate to increasing the stability

in the combustion of lean mixtures, which is the most important merit of matrix-stabilized

combustion on porous media.

LIST OF REFERENCES

[1]   S. Wood and A. T. Harris, "Porous burners for lean-burn applications," *Progress in Energy and Combustion Science,* vol. 34, pp. 667-684, 2008.

[2]   J. Howell, M. Hall, and J. Ellzey, "Combustion of hydrocarbon fuels within porous inert media," *Progress in Energy and Combustion Science,* vol. 22, pp. 121-145, 1996.

[3]   M. A. Mujeebu, M. Z. Abdullah, M. Z. A. Bakar, A. A. Mohamad, R. M. N. Muhad, and M. K. Abdullah, "Combustion in porous media and its applications – A comprehensive survey," *Journal of Environmental Management,* vol. 90, pp. 2287-2312, 2009.

[4]   T. TAKENO and K. SATO, "An excess enthalpy flame theory," *Combustion Science and Technology,* vol. 20, pp. 73-84, 1979.

[5]   A. Mohamad, "11 COMBUSTION IN POROUS MEDIA: FUNDAMENTALS AND APPLICATIONS," *Transport phenomena in porous media III,* vol. 3, p. 287, 2005.

[6]   Y. Huang, C. Chao, and P. Cheng, "Effects of preheating and operation conditions on combustion in a porous medium," *International Journal of Heat and Mass Transfer,* vol. 45, pp. 4315-4324, 2002.

[7]   L. Kennedy, A. Saveliev, J. Bingue, and A. Fridman, "Filtration combustion of a methane wave in air for oxygen-enriched and oxygen-depleted environments," *Proceedings of the Combustion Institute,* vol. 29, pp. 835-841, 2002.

[8]   V. Babkin, "Filtrational combustion of gases. Present state of affairs and prospects," *Pure and Applied Chemistry,* vol. 65, pp. 335-335, 1993.

[9]   S. Zhdanok, L. A. Kennedy, and G. Koester, "Superadiabatic combustion of methane air mixtures under filtration in a packed bed," *Combustion and Flame,* vol. 100, pp. 221-231, 1995.

[10]   S. R. Turns, *An introduction to combustion* vol. 499: McGraw-Hill New York, 1996.

[11]   F. J. Weinberg, "Advanced combustion methods," Imperial College of Science and Technology, London1986.

[12]   D. Dunn-Rankin, *Lean combustion: technology and control*: Access Online via Elsevier, 2011.

[13]   I. Glassman and R. Yetter, *Combustion*: Academic press, 2008.

[14]   W. M. Mathis and J. L. Ellzey, "Flame stabilization, operating range, and emissions for a methane/air porous burner," *Combustion Science and Technology,* vol. 175, pp. 825-839, 2003.

[15]   F. Weinberg, "Combustion temperatures: the future?," *Nature,* vol. 233, pp. 239-241, 1971.

[16]   M. A. Mujeebu, M. Abdullah, M. Bakar, A. Mohamad, and M. Abdullah, "Applications of porous media combustion technology–a review," *Applied Energy,* vol. 86, pp. 1365-1375, 2009.

[17]   S. Jugjai and V. Nungniyom, "Cyclic operation of porous combustor-heater (PCH)," *Fuel,* vol. 88, pp. 553-559, 2009.

[18]   A. Oliveira and M. Kaviany, "Nonequilibrium in the transport of heat and reactants in combustion in porous media," *Progress in Energy and Combustion Science,* vol. 27, pp. 523-545, 2001.

[19]   D. Trimis and F. Durst, "Combustion in a porous medium-advances and applications," *Combustion Science and Technology,* vol. 121, pp. 153-168, 1996.

[20] Y. Kotani and T. Takeno, "An experimental study on stability and combustion characteristics of an excess enthalpy flame," in *Symposium (International) on Combustion*, 1982, pp. 1503-1509.

[21] R. Mital, J. Gore, and R. Viskanta, "A study of the structure of submerged reaction zone in porous ceramic radiant burners," *Combustion and Flame,* vol. 111, pp. 175-184, 1997.

[22] J. Bingue, A. Saveliev, A. Fridman, and L. Kennedy, "NOx AND CO EMISSIONS OF METHANE/AIR FILTRATION COMBUSTION WAVES," *m th3 213j: csmury (355 2000),* p. 1266, 2000.

[23] L. A. Kennedy and A. Saveliev, "Superadiabatic combustion in porous media: wave propagation, instabilities, new type of chemical reactor," *International Journal of Fluid Mechanics Research,* vol. 22, 1995.

[24] C. Tierney and A. Harris, "Materials Design and Selection Issues in Ultra-Lean Porous Burners," *Journal of the Australian Ceramic Society Volume,* vol. 45, pp. 20-29, 2009.

[25] O. Pickenäcker, K. Pickenäcker, K. Wawrzinek, D. Trimis, W. Pritzkow, C. Müller, P. Goedtke, U. Papenburg, J. Adler, and G. Standke, "Innovative ceramic materials for porous-medium burners," *Interceram,* vol. 48, pp. 326-330, 1999.

[26] C.-H. Zheng, L.-M. Cheng, T. Li, Z.-Y. Luo, and K.-F. Cen, "Filtration combustion characteristics of low calorific gas in SiC foams," *Fuel,* vol. 89, pp. 2331-2337, 2010.

[27] C. Keramiotis, B. Stelzner, D. Trimis, and M. Founti, "Porous burners for low emission combustion: An experimental investigation," *Energy,* vol. 45, pp. 213-219, 2012.

[28] K. Dobrego, N. Gnesdilov, S. Lee, and H. Choi, "Lean combustibility limit of methane in reciprocal flow filtration combustion reactor," *International Journal of Heat and Mass Transfer,* vol. 51, pp. 2190-2198, 2008.

[29]   S. Afsharvahid, B. Dally, and F. Christo, "On The Stabilisation Of Ultra Lean Methane and Propane Flames in Porous Media," in *The Fourth Asia-Pacific Conference on Combustion*, 2003.

[30]   L. A. Kennedy, J. P. Bingue, A. V. Saveliev, A. Fridman, and S. I. Foutko, "Chemical structures of methane-air filtration combustion waves for fuel-lean and fuel-rich conditions," *Proceedings of the Combustion Institute,* vol. 28, pp. 1431-1438, 2000.

[31]   F. C. Christo, B. Dally, P. Lanspeary, S. Afsharvahid, and S. Joseph, "Development of porous burner technology for ultra-lean combustion systems," Final Technical Report-SENRAC Grant 03/00-South Australian State Energy Research Advisory Committee2002.

[32]   J. G. Hoffmann, R. Echigo, H. Yoshida, and S. Tada, "Experimental study on combustion in porous media with a reciprocating flow system," *Combustion and Flame,* vol. 111, pp. 32-46, 1997.

[33]   J. Hoffmann, R. Echigo, S. Tada, and H. Yoshida, "Analytical study on flame stabilization in reciprocating combustion in porous media with high thermal conductivity," in *Symposium (International) on Combustion*, 1996, pp. 2709-2716.

[34]   K. Hanamura, R. Echigo, and S. A. Zhdanok, "Superadiabatic combustion in a porous medium," *International Journal of Heat and Mass Transfer,* vol. 36, pp. 3201-3209, 1993.

[35]   A. Lane. (2013, 6/14/2013). *Crimson Catalysis*.

[36]   L. Pfefferle and W. Pfefferle, "Catalysis in combustion," *Catalysis Reviews Science and Engineering,* vol. 29, pp. 219-267, 1987.

[37] M. F. Zwinkels, S. G. Järås, P. G. Menon, and T. A. Griffin, "Catalytic materials for high-temperature combustion," *Catalysis Reviews—Science and Engineering,* vol. 35, pp. 319-358, 1993.

[38] F. Martinez-Ortega, C. Batiot-Dupeyrat, G. Valderrama, and J.-M. Tatibouët, "Methane catalytic combustion on La-based perovskite catalysts," *Comptes Rendus de l'Académie des Sciences - Series IIC - Chemistry,* vol. 4, pp. 49-55, 1/1/ 2001.

[39] T. Choudhary, S. Banerjee, and V. Choudhary, "Catalysts for combustion of methane and lower alkanes," *Applied Catalysis A: General,* vol. 234, pp. 1-23, 2002.

[40] S. Cimino, L. Lisi, R. Pirone, G. Russo, and M. Turco, "Methane combustion on perovskites-based structured catalysts," *Catalysis Today,* vol. 59, pp. 19-31, 2000.

[41] A. Qi, S. Wang, G. Fu, C. Ni, and D. Wu, "La–Ce–Ni–O monolithic perovskite catalysts potential for gasoline autothermal reforming system," *Applied Catalysis A: General,* vol. 281, pp. 233-246, 2005.

[42] F. Martinez-Ortega, C. Batiot-Dupeyrat, G. Valderrama, and J.-M. Tatibouët, "Methane catalytic combustion on La-based perovskite catalysts," *Comptes Rendus de l'Académie des Sciences-Series IIC-Chemistry,* vol. 4, pp. 49-55, 2001.

[43] H. Tanaka and M. Misono, "Advances in designing perovskite catalysts," *Current Opinion in Solid State and Materials Science,* vol. 5, pp. 381-387, 2001.

[44] S.-W. C. Ryan O'Hayre, Whitney Colella, Fritz B. Prinz, *Fuel Cell Fundamentals*, Second ed. New York: John Wiley & Sons, 2009.

[45] A. S. Bhalla, R. Guo, and R. Roy, "The perovskite structure – a review of its role in ceramic science and technology," *Materials Research Innovations,* vol. 4, pp. 3-26, 2000.

[46]   J. William D. Callister and D. G. Rethwisch, *Materials Science and Engineering An Introduction*, Eighth ed., 2009.

[47]   V. Milt, R. Spretz, M. Ulla, E. Lombardo, and J. G. Fierro, "The nature of active sites for the oxidation of methane on La-based perovskites," *Catalysis letters,* vol. 42, pp. 57-63, 1996.

[48]   R. Voorhoeve, D. Johnson, J. Remeika, and P. Gallagher, "Perovskite oxides: Materials science in catalysis," *Science,* vol. 195, pp. 827-833, 1977.

[49]   N. K. Labhsetwar, A. Watanabe, T. Mitsuhashi, and H. Haneda, "Thermally stable ruthenium-based catalyst for methane combustion," *Journal of Molecular Catalysis A: Chemical,* vol. 223, pp. 217-223, 2004.

[50]   M. Lee, J. Jun, J. Jung, Y. Kim, and S. Lee, "Catalytic Activities of Perovskite-type LaBO~ 3 (B= Fe, Co, Ni) Oxides for Partial Oxidation of Methane," *BULLETIN-KOREAN CHEMICAL SOCIETY,* vol. 26, p. 1591, 2005.

[51]   C. Batiot-Dupeyrat, F. Martinez-Ortega, M. Ganne, and J. Tatibouët, "Methane catalytic combustion on La-based perovskite type catalysts in high temperature isothermal conditions," *Applied Catalysis A: General,* vol. 206, pp. 205-215, 2001.

[52]   J. Suntivich, H. A. Gasteiger, N. Yabuuchi, and Y. Shao-Horn, "Electrocatalytic measurement methodology of oxide catalysts using a thin-film rotating disk electrode," *Journal of The Electrochemical Society,* vol. 157, pp. B1263-B1268, 2010.

[53]   J. Suntivich, H. A. Gasteiger, N. Yabuuchi, H. Nakanishi, J. B. Goodenough, and Y. Shao-Horn, "Design principles for oxygen-reduction activity on perovskite oxide catalysts for fuel cells and metal–air batteries," *Nature chemistry,* vol. 3, pp. 546-550, 2011.

[54]   J. O. M. Bockris and T. Otagawa, "The electrocatalysis of oxygen evolution on perovskites," *Journal of The Electrochemical Society,* vol. 131, pp. 290-302, 1984.

[55]   R. F. Savinell, "Oxygen-reduction catalysts: Picking perovskites," *Nature chemistry,* vol. 3, pp. 501-502, 2011.

[56]   F. Weinberg, D. Rowe, G. Min, and P. Ronney, "On thermoelectric power conversion from heat recirculating combustion systems," *Proceedings of the Combustion Institute,* vol. 29, pp. 941-947, 2002.

[57]   F. J. Weinberg, "Combustion in heat-recirculating burners," *Advanced Combustion Methods,* pp. 183-236, 1986.

[58]   R. Decher, *Direct Energy Conversion: fundamentals of electric power production*: Oxford University Press Oxford, 1997.

[59]   S. Misture and D. Edwards, "HIGH-TEMPERATURE OXIDE THERMOELECTRICS," *American Ceramics Society Bulletin,* vol. 91, pp. 24-27, 2012.

[60]   K. Uchida, S. Takahashi, K. Harii, J. Ieda, W. Koshibae, K. Ando, S. Maekawa, and E. Saitoh, "Observation of the spin Seebeck effect," *Nature,* vol. 455, pp. 778-781, 2008.

[61]   K. Hanamura, T. Kumano, and Y. Iida, "Electric power generation by super-adiabatic combustion in thermoelectric porous element," *Energy,* vol. 30, pp. 347-357, 2005.

[62]   C.-W. Park and M. Kaviany, "Combustion-thermoelectric tube," *TRANSACTIONS-AMERICAN SOCIETY OF MECHANICAL ENGINEERS JOURNAL OF HEAT TRANSFER,* vol. 122, pp. 721-729, 2000.

[63]   K. T. Mueller, O. Waters, V. Bubnovich, N. Orlovskaya, and R.-H. Chen, "Super-adiabatic combustion in Al 2 O3 and SiC coated porous media for thermoelectric power conversion," *Energy,* vol. 56, pp. 108-116, 2013.

[64]   J. Hudson, M. Robayo, J. Rodriguez, and E. Vinueza, "Senior Design Final Report "Porous Combustor Thermoelectric Generator"," University of Central Florida2011.

[65]   M. Michiel, E. Solares, and L. Streter, ""Thermoelectric Module Experiment", A Measurements II project commissioned by Manuel D. Robayo," University of Central Florida2012.

[66]   W. Zhu and S. Deevi, "Development of interconnect materials for solid oxide fuel cells," *Materials Science and Engineering: A,* vol. 348, pp. 227-243, 2003.

[67]   A. Zuev, L. Singheiser, and K. Hilpert, "Defect structure and isothermal expansion of A-site and B-site substituted lanthanum chromites," *Solid State Ionics,* vol. 147, pp. 1-11, 2002.